




Article

Efficacy of Deferoxamine Mesylate in Serum and Serum-Free Media: Adult Ventral Root Schwann Cell Survival Following Hydrogen Peroxide-Induced Cell Death

Yee Hang Ethan Ma ¹, Abhinay R. Putta ², Cyrus H. H. Chan ², Stephen R. Vidman ³ , Paula Monje ⁴ 
and Giles W. Plant ^{1,*} 

¹ Department of Neuroscience and Chronic Brain Injury Program, The Ohio State University, Columbus, OH 43210, USA; yeehangethan.ma@osumc.edu

² Department of Neuroscience, The Ohio State University, Columbus, OH 43210, USA; abhinay.putta@osumc.edu (A.R.P.); hohin.chan@osumc.edu (C.H.H.C.)

³ Department of Neuroscience and Neuroscience Graduate Program, The Ohio State University, Columbus, OH 43210, USA; stephen.vidman@osumc.edu

⁴ Department of Neurosurgery, University of Kentucky, Lexington, KY 40506, USA; pmonje@uky.edu

* Correspondence: giles.plant@osumc.edu

Abstract: Schwann cell (SC) transplantation shows promise in treating spinal cord injury as a pro-regenerative agent to allow host endogenous neurons to bridge over the lesion. However, SC transplants face significant oxidative stress facilitated by ROS in the lesion, leading to poor survival. deferoxamine mesylate (DFO) is a neuroprotective agent shown to reduce H₂O₂-induced cell death in serum-containing conditions. Here we show that DFO is not necessary to induce neuroprotection under serum-free conditions by cell survival quantification and phenotypic analysis via immunohistochemistry, Hif1 α and collagen IV quantification via whole cell corrected total cell fluorescence, and cell death transcript changes via RT-qPCR. Our results indicate survival of SC regardless of DFO pretreatment in serum-free conditions and an increased survival facilitated by DFO in serum-containing conditions. Furthermore, our results showed strong nuclear expression of Hif1 α in serum-free conditions regardless of DFO pre-treatment and a nuclear expression of Hif1 α in DFO-treated SCs in serum conditions. Transcriptomic analysis reveals upregulation of autophagy transcripts in SCs grown in serum-free media relative to SCs in serum conditions, with and without DFO and H₂O₂. Thus, indicating a pro-repair and regenerative state of the SCs in serum-free conditions. Overall, results indicate the protectiveness of CDM in enhancing SC survival against ROS-induced cell death in vitro.

Keywords: Schwann cells; spinal cord injury; deferoxamine mesylate; oxidative stress; transplantation



Academic Editor: Hakan Aldskogius

Received: 5 February 2025

Revised: 12 March 2025

Accepted: 14 March 2025

Published: 20 March 2025

Citation: Ma, Y.H.E.; Putta, A.R.; Chan, C.H.H.; Vidman, S.R.; Monje, P.; Plant, G.W. Efficacy of Deferoxamine Mesylate in Serum and Serum-Free Media: Adult Ventral Root Schwann Cell Survival Following Hydrogen Peroxide-Induced Cell Death. *Cells* **2025**, *14*, 461. <https://doi.org/10.3390/cells14060461>

Copyright: © 2025 by the authors. Licensee MDPI, Basel, Switzerland. This article is an open access article distributed under the terms and conditions of the Creative Commons Attribution (CC BY) license (<https://creativecommons.org/licenses/by/4.0/>).

1. Introduction

Spinal cord injury (SCI) is a severe, life-altering condition affecting over 500,000 individuals annually, predominantly resulting from preventable causes such as motor vehicle accidents and violence [1]. A hallmark of SCI is axon degeneration, where the synaptic connections between neurons are disrupted, leading to loss of function and further neurological complications [2–4]. Cellular transplantation therapies have emerged as a promising approach for axon regeneration, with autologous Schwann cell (SC) transplants currently being evaluated in clinical trials for their efficacy in treating cervical and thoracic SCI [5–14]. Originally proposed by David and Aguayo in 1981, peripheral nerve transplants were

shown to promote regeneration within the central nervous system by grafting peripheral nerve tissues, which induced axonal regrowth in focal injuries [14]. Since then, SCs have been characterized as peripheral glial cells and have shown considerable regenerative potential in SCI models, with numerous preclinical studies highlighting their capability to facilitate axon regeneration [8–14]. Compared to other transplant paradigms such as neural progenitor cell (NPC) transplants [15–17], SCs offer several advantages. As SCs are mature cells, the risk of spontaneous differentiation into unintended cell types and the formation of ectopic colonies seen in neural stem cell transplantations are eliminated [18]. Furthermore, the autologous nature of the transplants limits the need for immunosuppression following transplantation [11,19]. There are also standardized and straightforward methods to isolate and characterize SCs from a patient's peripheral nerves, making them an accessible and consistent candidate for cellular transplantation therapy [20,21].

Nonetheless, SC transplants face several challenges, particularly the acute death of transplanted cells caused by oxidative stress in the host spinal cord following injury. Reactive oxygen species (ROS) such as hydrogen peroxide, hydroxyl radicals, and superoxide anion radicals have been shown to induce oxidative stress and mediate cell death in spinal cord injury [22]. Thus, the efficacy of cellular transplant therapies has been limited due to the acute cell death that occurs post-transplantation. To address the issue, recent strategies have been focused on preconditioning SC with various pharmaceutical agents prior to transplantation [23–26].

One such agent of interest is deferoxamine mesylate (DFO) [22,26]. Mechanistically, DFO acts as an iron (Fe^{2+}) chelator, thus inhibiting the function of HIF-PHDs, hypoxia-inducible factor-prolyl hydroxylase domain proteins, and other Fe^{2+} , O_2 , and 2-oxoglutarate-dependent enzymes that mark HIF, hypoxia-inducible factor, proteins for proteasomal degradation [23,27,28]. This inhibition results in the stabilization of HIFs, allowing them to accumulate and activate their downstream effects. HIF stabilization then increases the expression of hypoxia response element (HRE) genes, which creates a cytoprotective environment and decreases cell death in hypoxic conditions. However, it remains unclear how DFO affects SC protein expression, phenotype, morphology, survivability, and transcriptome in response to ROS-induced cell death. While it is ascertained that DFO provides protection against ferroptosis [29,30], questions remain on whether it is effective in preventing acute cell death mediated by ROS.

The efficacy of DFO as a protective agent against oxidative stress has previously been demonstrated in serum-containing conditions, where it has shown potential to stabilize the expression of hypoxia-inducible factor (HIF) family proteins and protect cells under hypoxic conditions, thereby reducing ROS-induced cell death [23,27,31,32]. However, the relevance of serum-based treatments to modern clinical practices is limited, due to the inherent variability in the composition of serum [33–36]. A serum-free approach with predefined and consistent composition offers a more reliable alternative, enabling reproducible and clinically relevant results. Hence, it is important to evaluate the effects of DFO on SCs in serum-free conditions to determine whether its protective properties remain effective and clinically relevant.

The goal of the study is to characterize the effectiveness of DFO in increasing the survival of Schwann cells (SCs) upon hydrogen peroxide-induced cell death in an in vitro environment designed to simulate clinical transplant conditions. We hypothesized that SCs pre-treated with DFO would exhibit increased survival in ROS-induced cell death in serum-containing conditions. Additionally, we hypothesized that the neuroprotective effects of DFO would persist in serum-free conditions, which eliminates the need for patient serum extraction while decreasing serum-facilitated SC variation in vivo. We examined the efficacy of DFO in both serum-containing and serum-free conditions (abbreviations and

components of medias shown in Supplementary Table S1) and assessed our results through phenotypic staining, cell count, whole cell corrected total cell fluorescence analysis, and RT-qPCR cell death transcriptomics. Our findings show a significant increase in cellular survival upon hydrogen peroxide challenge at 62.5 μ M in populations pre-treated with DFO only in serum-containing conditions. Furthermore, we observed that serum-free media exhibited inherent neuroprotective properties, presenting it as a viable alternative to serum-containing media altogether.

2. Materials and Methods

2.1. Generation and Expansion of Schwann Cell Culture

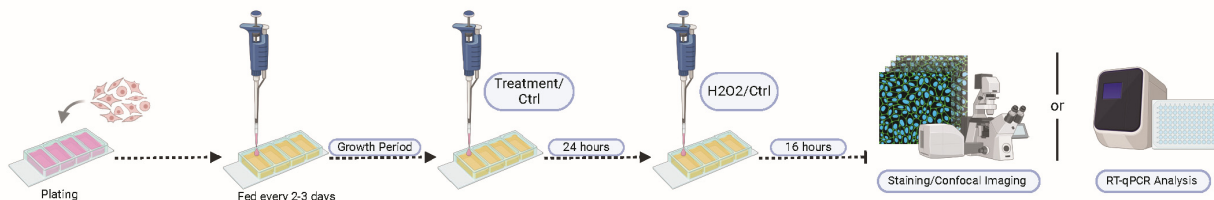
Schwann cells (SCs) were isolated from the ventral roots of 6-month-old adult GFP transgenic Sprague Dawley rats according to our established protocols for SC culturing from immediately dissociated nerve tissues [37]. The initial cell harvest was plated in the form of droplets directly onto PLL-laminin-coated dishes and expanded in DMEM medium supplemented with 10% FBS, heregulin (10 nM), and forskolin (2 μ M) up until confluency. Cells were subsequently lifted from their dishes by trypsinization and purified of contaminating fibroblasts by MACS sorting after incubation with Thy1.1 antibodies, as described in Ravelo et al. [37]. The purified SCs were expanded up to passage-1 (P1) in the abovementioned medium for the creation of cryogenic stocks [37]. These stocks were maintained in liquid nitrogen until use. Prior to the experiment, P1 SCs were expanded in D10S 3F (Supplementary Table S1). During expansion, SCs were cultured in poly-L-lysine (PLL, Millipore Sigma P6282, St. Louis, MO, USA) coated 100 mm Corning-treated tissue culture dishes and fed with 7 mL of CDM 3F (Supplementary Table S1) every 2–3 days. Once the desired confluency (approx. 5 million cells per plate) and maturation state were achieved by visual confirmation of cell swirling, SCs were either split into new 100 mm Corning-treated tissue culture dishes or split into experimental conditions. SCs were detached using 0.05% trypsin-EDTA (Gibco 25300054, Waltham, MA, USA) and seeded into PLL-coated four-well chamber slides (Nunc Lab-Tek II Chamber Slide System, ThermoFisher, Waltham, MA, USA), at 50,000 cells per well, for immunocytochemistry experiments and fed with 350 μ L CDM 3F per well every 2–3 days until the start of the experiment (Section 2.3). For RT-qPCR experiments, SCs were plated into 60 mm PLL-coated TPP tissue culture dishes (TPP 93060, Trasadingen, Switzerland) at 450,000 cells/plate and fed with 5 mL of CDM 3F every 2–3 days until treatment (Section 2.4). All SCs were cultured in a 5% CO₂, 37 °C incubator except for the cells at passage-zero (P0) and P1, which were cultured in a CO₂ incubator set up at 9% CO₂. P2-P5 SCs were used for all experiments. The purity of the SC populations was >98% at P1, as judged by co-immunostaining with S100B and Thy1.1 antibodies. SCs from ventral roots were highly proliferative and visually indistinguishable from the ones derived from the sciatic nerve [38].

2.2. Experimental Treatments and Timeline

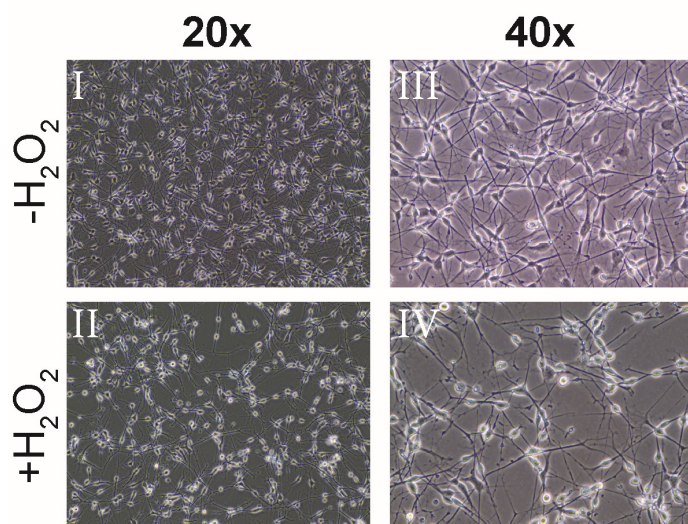
SCs were plated onto four-well chamber slides for phenotypic staining and subsequently onto 60 mm PLL-coated TPP tissue culture dishes for cell death transcriptomics analysis. All SCs are initially cultured in serum containing CDM 3F media until the desired confluency is reached by visual confirmation of swirling. Prior to the 62.5 μ M H₂O₂ challenge or sham, SCs were treated with their respective pre-treatment conditions (Supplementary Table S2) for 24 h, followed by a 16-h exposure to 62.5 μ M H₂O₂ in base media. 3F signaling was cleared for selected groups (Sections 3.3 and 3.4 comparing SCs serum and serum-free. SCs were fed with their respective base medium for 4 days;. For sham, SCs were refed with base media only. After the treatment period, SCs were either fixed with 4% paraformaldehyde for subsequent phenotypic staining and density analysis

or harvested as cell pellets for RT-qPCR cell death transcriptomics analysis (Section 2.4). Figure 1A illustrates the experimental timeline, and Figure 1B,C shows the effect of the 16-h exposure to 62.5 μM H_2O_2 on SCs. Figure 2A, Figure 3A, Figure 4A and Figure 7A show the timeline of the media condition changes during the experiments.

A Experimental Design



B Serum Medium: D10S



C Serum-Free Medium: CDM

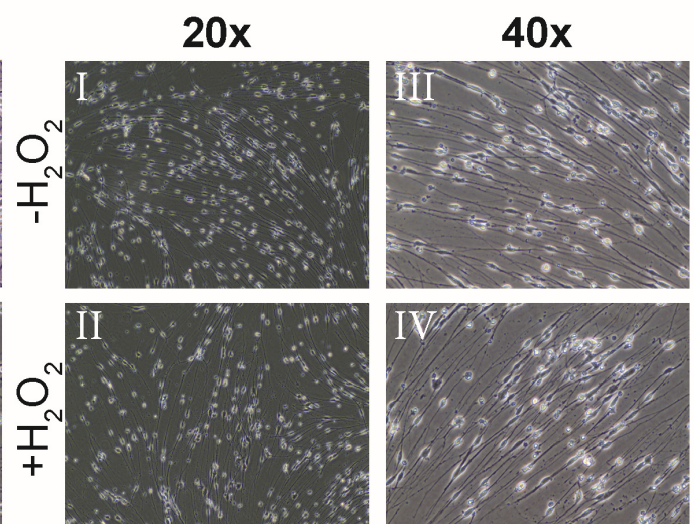


Figure 1. Schematic of experimental design and Schwann cell cultures. (A) Schematic of the experiments. Timepoints of treatments and hydrogen peroxide challenge. (B) Representative brightfield images of Schwann cells 16 h following hydrogen peroxide challenge (B(III,IV)) or sham (B(I,II)) in serum-containing medium. (B(I,III)) shows a 20 \times image, and (B(II,IV)) shows a 40 \times image. (C) Representative brightfield images of Schwann cells 16 h following hydrogen peroxide challenge (C(III,IV)) or sham (C(I,II)) in serum-free medium. (C(I,III)) shows a 20 \times image and (C(II,IV)) shows a 40 \times image. All images are taken on the Invitrogen EVOS XL CORE inverted brightfield microscope using EAcro 40 \times LWD PH, 0.65 NA/3.1 WD (AMEP4635), and Achro 20 \times LWD PH, 0.40 NA/6.8 WD (AMEP4934) objectives.

2.3. Immunofluorescence Staining

16 h after the H_2O_2 challenge, SCs were fixed via a 15 min incubation with approximately 300 μL of chilled 4% paraformaldehyde at room temperature. After PFA incubation, SCs were washed three times with 1X PB and stored at +4 $^\circ\text{C}$ with phosphate buffer (PB) until immunostaining. We stained SCs with GFAP (Chicken, 1:1000, Aves GFAP, Davis, CA, USA), P75 (Rabbit, 1:400, Bioss BS-0161R, Woburn, MA, USA), HiF1 α (Rabbit, 1:500, Sigma Aldrich SAB5701087, St. Louis, MO, USA), and Collagen IV (Rabbit, 1:400, Rockland 600-401-106-0.1, Pottstown, PA, USA) primary antibodies. Secondary antibodies used were from Jackson Immuno (West Grove, PA, USA) and used at 1:800; we used donkey anti-chicken AlexaFluor 488 (703-546-155) and donkey anti-rabbit cy3 (711-166-152). SCs were incubated at room temperature with primary antibody in blocking solution: 90% 1X

phosphate buffer (PB), 10% Donkey Serum (Lampire 7332100, Pipersville, PA, USA), and 0.2% Triton X-100 (Sigma Aldrich X100, St. Louis, MO, USA), for 2 h, then washed with 1X PB three times. SCs are then incubated with secondary antibody in blocking solution at room temperature for 45 min in the dark. Cells are subsequently washed with 1X PB three times and cover slipped with Prolong Gold or Diamond Antifade Mountant with DAPI (Invitrogen, Waltham, MA, USA).

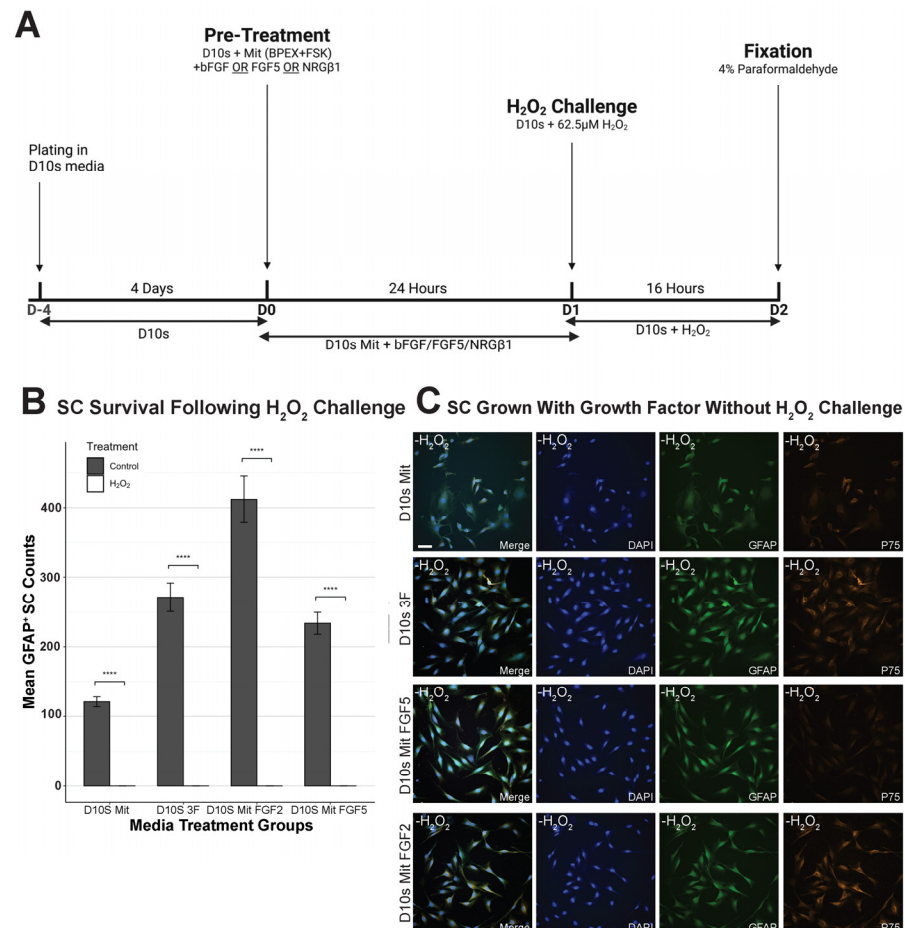


Figure 2. Growth factors do not protect against H_2O_2 -induced Schwann cell death in vitro. (A) Schematic of the experiment. SCs were grown for 4 days on four-well chambers prior to exposure to treatment conditions. (B) Quantification of cellular survival in sham versus hydrogen peroxide challenged SCs in D10s Mit, D10s 3F, and D10s Mit + FGF2, D10s Mit + FGF5 shows no effect of growth factors in increasing SC survival. (C) Representative images of sham SCs in different conditions. Images are taken at x40. Channels: DAPI (405, blue), GFAP (488, green), P75 (Cy3, orange). Scale bar = 50 μ m. * ($p \leq 0.05$), ** ($p \leq 0.01$), *** ($p \leq 0.001$), **** ($p \leq 0.0001$).

2.4. Confocal Microscopy

All imaging was performed on a Nikon AXR confocal microscope using the Nikon NIS Elements software. The microscope is equipped with four lasers, ranging from 405 to 647. All cells were stained with DAPI (405) and their respective stains for qualitative and quantitative analysis (GFAP, P75, HIF1 α , Collagen IV). Image acquisition parameters are described in the sections below in the context of their application. Representative images taken for Figure 2 were taken using a Nikon APO LWD 40X WI IS DIC N2 (NA = 1.15, WD = 610 μ m) objective. Representative images for Figures 3–6 were taken using a Nikon APO LWD 20X WI IS (NA = 0.95, WD = 950 μ m).

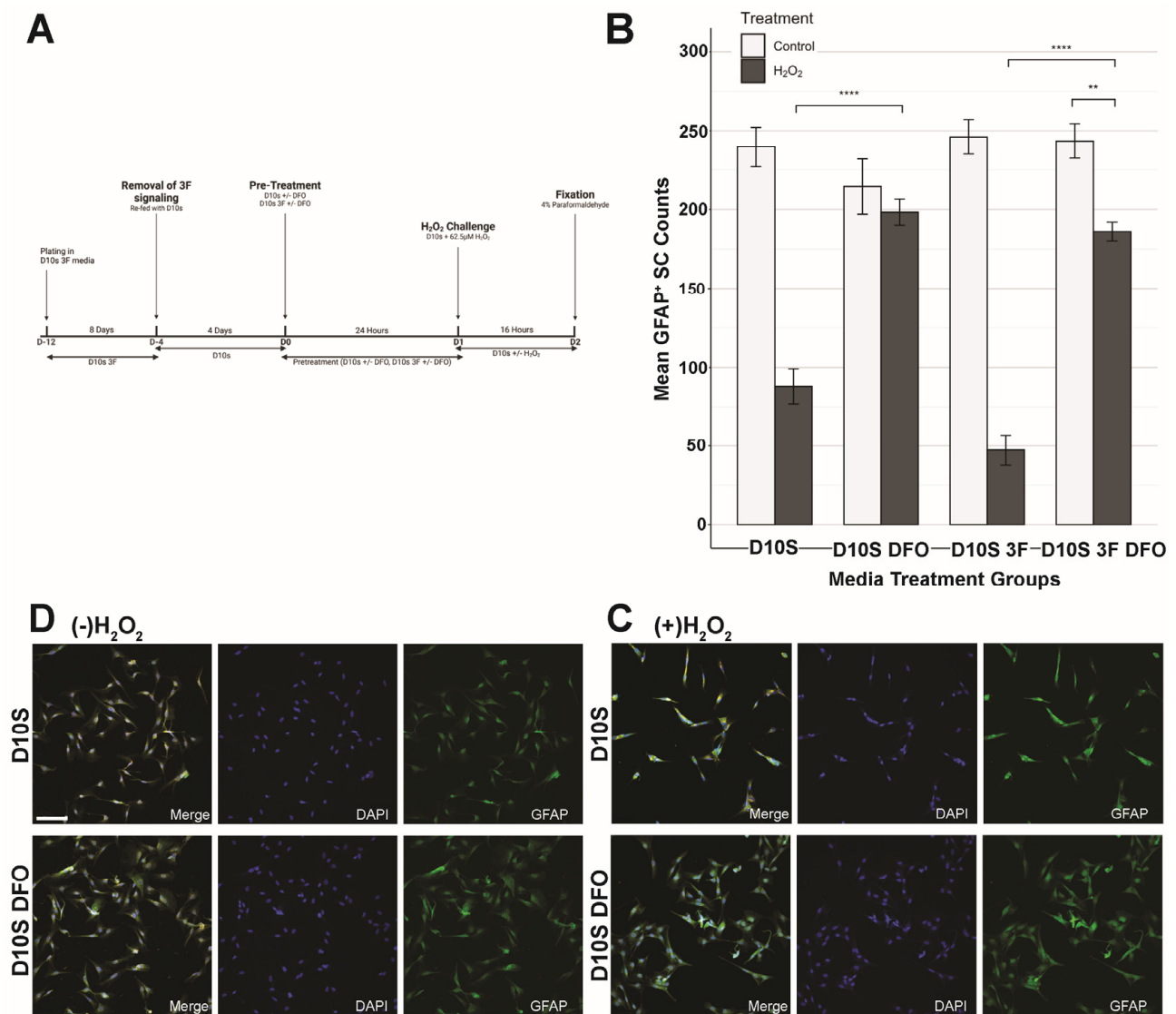


Figure 3. DFO increases Schwann cell survival in serum-containing medium. **(A)** Schematic of the experimental design. SCs were grown for 8 days in D10S 3F medium to eliminate fibroblasts in culture and promote SC survival and proliferation. **(B)** Quantification of GFAP + SC nucleus 16 h following sham or hydrogen peroxide challenge. D10S + DFO survival is significantly higher compared to D10S. D10S 3F + DFO survival is significantly higher than D10S 3F. **(C)** Representative images of D10S and D10S + DFO following 16 h of 62.5 μM hydrogen peroxide challenge. Channels: DAPI (405/blue), GFAP (488, green), Hif1α (cy3, orange). **(D)** Representative images of D10S and D10S + DFO following 16 h of sham. Channels: DAPI (405/blue), GFAP (488, green), Hif1α (cy3, orange). Hif1α staining is shown in Figure 5. Images taken at 20× magnification and 1.5× zoom. Scale bar = 100 μm. * ($p \leq 0.05$), ** ($p \leq 0.01$), *** ($p \leq 0.001$), **** ($p \leq 0.0001$).

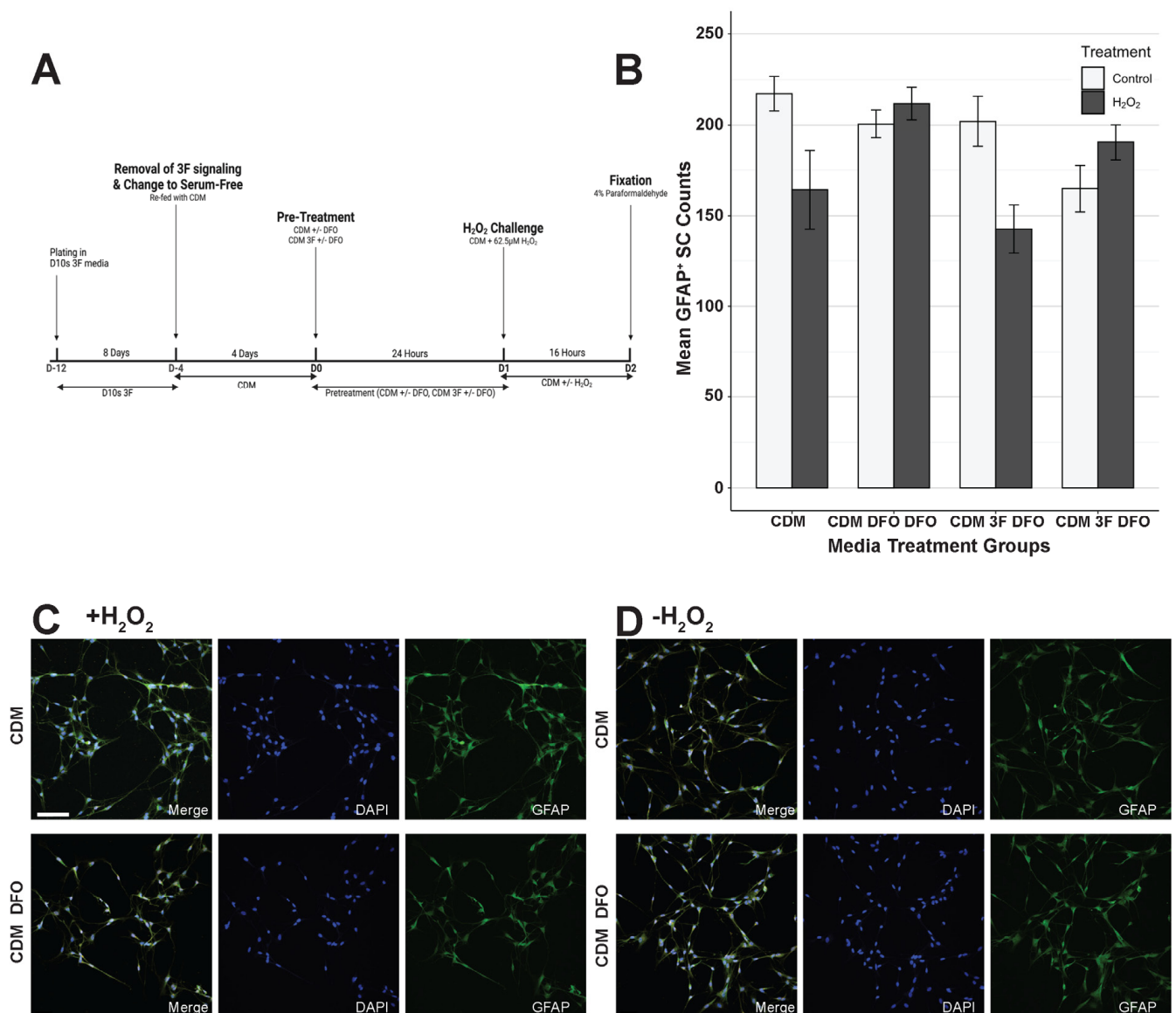


Figure 4. Serum-free medium protects Schwann cells in H₂O₂-induced cell death. **(A)** Schematic of the experiment. SCs were grown for 8 days in D10S 3F medium to eliminate fibroblasts in culture and promote SC survival and proliferation. **(B)** Quantification of GFAP + SC nucleus 16 h following sham or hydrogen peroxide challenge. CDM + DFO survival shows no significant increase compared to CDM. CDM 3F + DFO survival shows no significant difference compared to CDM 3F. **(C)** Representative images of CDM and CDM + DFO following 16 h of 62.5 μM hydrogen peroxide challenge. Channels: DAPI (405/blue), GFAP (488, green), Hif1α (cy3, orange). **(D)** Representative images of CDM 3F and CDM 3F + DFO following 16 h of sham. Channels: DAPI (405, blue), GFAP (488, green), Hif1α (cy3, orange). Hif1α staining is shown in Figure 5. Images taken at 20× magnification and 1.5× zoom. Scale = 100 μm. * ($p \leq 0.05$), ** ($p \leq 0.01$), *** ($p \leq 0.001$), **** ($p \leq 0.0001$).

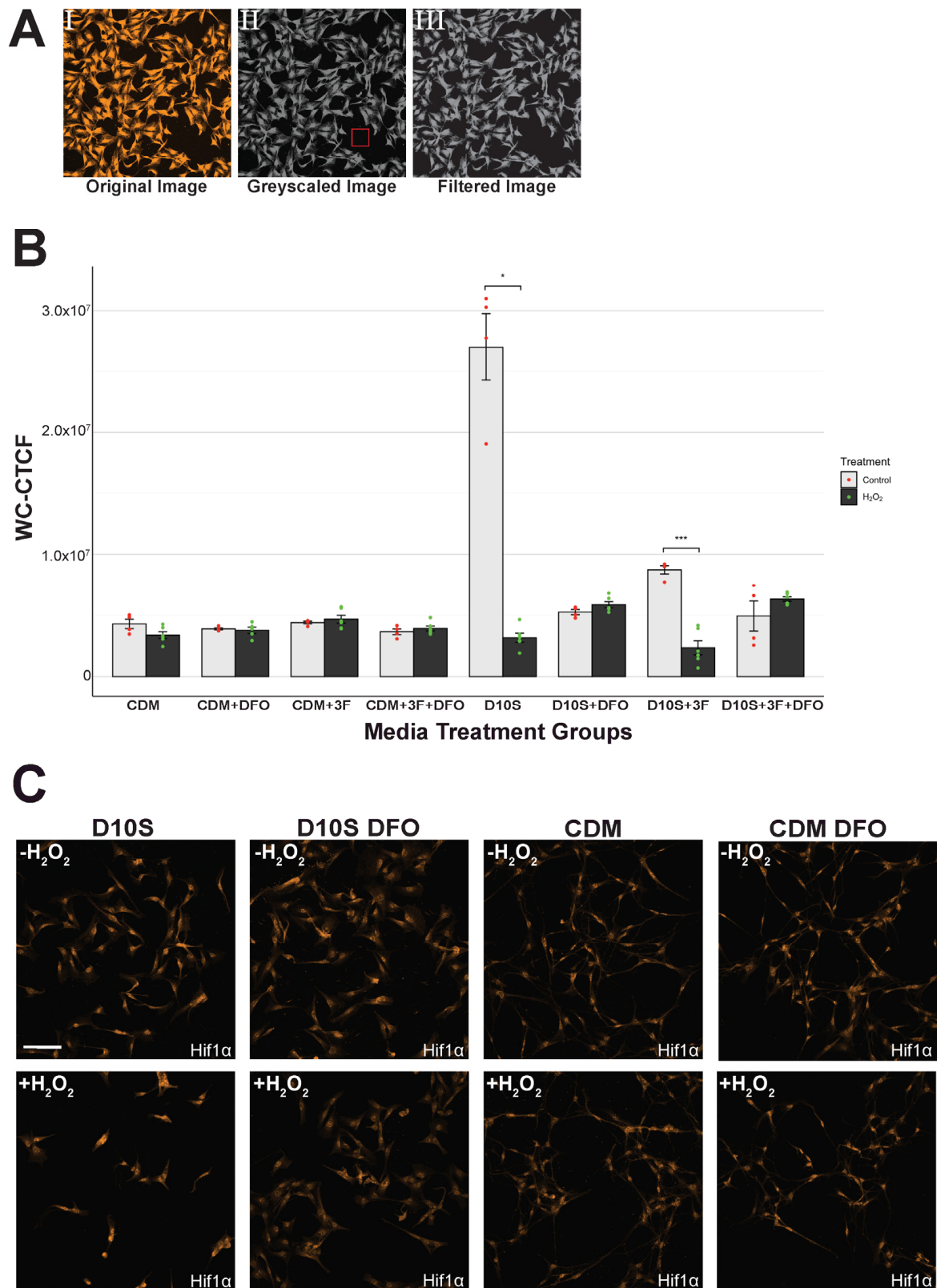


Figure 5. Hif1 α WC-CTCF reveals serum variability. (A) Representative process of fluorescence intensity quantification. (A(I)) Original image without processing. (A(II)) Greyscale image, box shows definition of “background”. (A(III)) Image after background filtering to eliminate noise. (B) Quantification of Hif1 α expression across groups. Statistics show high variability in serum groups with significant upregulation of Hif1 α in non-DFO pretreatment groups. (C) Representative images of Hif1 α expression across groups. Images taken at 20 \times magnification and 1.5 \times zoom. Scale = 100 μ m. * ($p \leq 0.05$), ** ($p \leq 0.01$), *** ($p \leq 0.001$), **** ($p \leq 0.0001$).

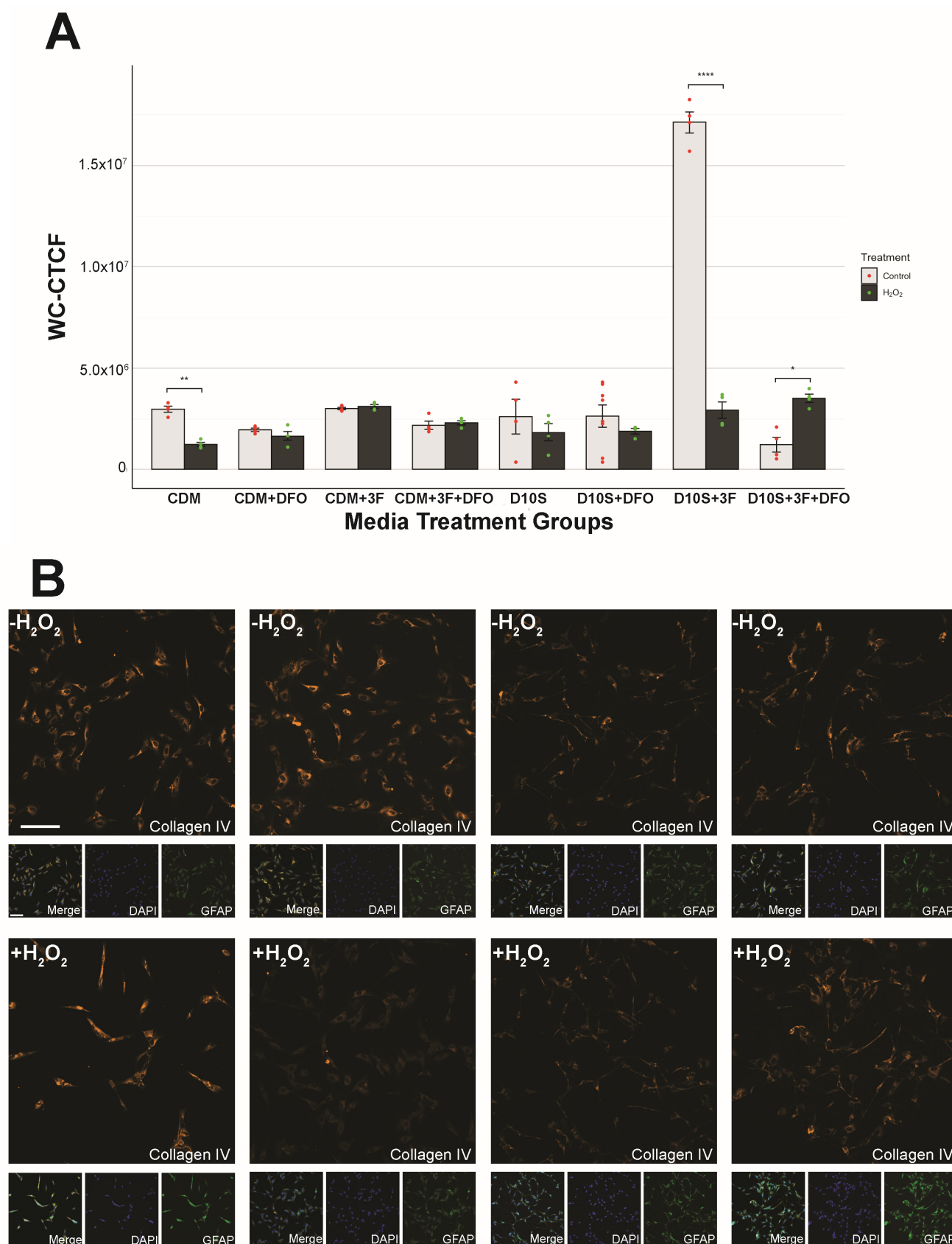


Figure 6. Collagen IV WC-CTCF shows Schwann cell states. **(A)** Quantification of collagen IV expression. *p* values for statistics are shown in Supplemental Table S7. **(B)** Representative images of collagen IV expression across groups following 16 h of 62.5 μ M hydrogen peroxide challenge or sham. Channels: Collagen IV (Cy3, orange), GFAP (488, green), DAPI (405, blue). Scale = 100 μ m. * ($p \leq 0.05$), ** ($p \leq 0.01$), *** ($p \leq 0.001$), **** ($p \leq 0.0001$).

2.5. Survival Quantification

Images taken from the wells were quantified using the NIH ImageJ software (ImageJ 2.14.0/1.54f; Java 1.8.0_322 [64 bit]). Quantification was semi-automated with human correction of software errors. Images were taken at 10× (NA = 0.45, WD = 4000 µm) magnification for each well. For each well, we randomly selected 3–4 fields. Using ImageJ, ND2 images were opened as grayscale images. The detection threshold was manually adjusted for all images to accurately highlight each individual DAPI stain. Images were then converted to binary images to remove background noise before being processed with the watershed algorithm to split any combined nucleus. DAPI nuclei were subsequently quantified using particle analysis with the size detection threshold set to 100 pixels to infinity. Quantification results were then compared with the original DAPI and GFAP stain manually to ensure accurate quantification and address any potential errors (e.g., splitting of a single nucleus, grouping of multiple nuclei, counting GFAP negative nuclei). Final quantifications were manually corrected for any software errors.

2.6. Hif1α and Collagen IV Quantification

Immunofluorescence images were obtained via confocal microscopy described in Section 2.5. Images were taken using a 20× objective (NA = 0.75, WD = 1000 µm), maintaining identical parameters for all Hif1α and Collagen IV scans as follows: laser power: 33, gain: 84.2, pinhole size: 1.2, zoom: 1×, z-stack: 50 µm, and step size: 2 µm. For Hif1α, we selected n = 6 per pre-treatment group (Supplementary Table S2). For collagen IV, we selected n = 4 per pre-treatment group. The images were then exported as ND2 files and further processed using a custom, semi-automated pipeline to quantify whole cell corrected total cell fluorescence (WC-CTCF) using FIJI/ImageJ software. In brief, ND2 files were split into single channels and compressed to maximum intensity projections (MIPs) for quantification. Then, the MIPs for Hif1α and Collagen IV were measured for total fluorescence in the image (integrated density), subtracted by the total background fluorescence. Utilizing this approach permits correction for size, density, or morphological differences between cells in their respective treatment groups. The formula used was CTCF = Integrated density – (total area × background intensity mean). We analyzed the whole cell fluorescence level to capture cytoplasmic and nuclear expression levels.

2.7. Statistical Analysis

All statistical analyses were conducted using the RStudio software 2024.04.2+764. Data were presented with error bars indicating standard error of the mean (SEM). Depending on data characteristics, either Welch’s one-way analysis of variance (Welch’s ANOVA) or standard ANOVA was used for F-tests. Post hoc comparisons were performed using Tukey’s HSD, Dunn’s Test, or Games–Howell test, as appropriate. $p \leq 0.05$ denotes statistical significance. Significance was also presented with the following notations: * ($p \leq 0.05$), ** ($p \leq 0.01$), *** ($p \leq 0.001$), **** ($p \leq 0.0001$). For RT-qPCR analysis, fold change was reported on the log2 scale, and comparative analyses were performed on GeneGlobe (Qiagen, Hilden, Germany).

2.8. Cell Death Transcriptomics

2.8.1. RNA Isolation

Selected groups (Supplementary Table S3) were chosen for transcriptomic analysis. Samples were lysed using the Qiashredder (Qiagen 79656, Hilden, Germany). RNA was isolated using the RNeasy Micro Kit (Qiagen 74004, Hilden, Germany) following the manufacturer’s instructions. Isolated RNA was subsequently stored at –80 °C until use. The quantity of extracted RNA was evaluated using Nanodrop 2000 (ThermoFisher, Waltham,

MA, USA) or BioTek Synergy HTX Multimode Reader (Agilent, Santa Clara, CA, USA), while the integrity was evaluated using Bioanalyzer 2100 (Agilent) for RNA Nano Chips (Agilent, Santa Clara, CA, USA) and TapeStation 4200 (Agilent, Santa Clara, CA, USA) for RNA ScreenTapes (Agilent, Santa Clara, CA, USA). RNA integrities were ensured to be of sufficient quality prior to PCR. 100 ng of total RNA was utilized for subsequent analysis within each group.

2.8.2. cDNA Synthesis

cDNA was synthesized using the RT2 First Strand Kit (Qiagen, 330404, Hilden, Germany) following the manufacturer's instructions. Samples were processed using the T100 Thermo-Cycler (BioRad, Hercules, CA, USA), starting with a 15-min incubation at 42 °C followed by a 5 min denaturation at 95 °C. Synthesized cDNA was stored at −20 °C until use. The quality and quantity of synthesized strands were evaluated using a Nanodrop 2000 (ThermoFisher, Waltham, MA, USA).

2.8.3. qPCR

The 96-well RT2 Profiler PCR Array Rat Cell Death PathwayFinder (Qiagen 330231 PARN-212ZA, Hilden, Germany) was used to detect expression levels of 84 targeting genes and 5 control genes (Supplementary Table S4). Selected genes were essential for the central mechanisms of cellular death, spanning apoptosis, autophagy, and necrosis. Following the manufacturer's instructions, cDNA was mixed with RT2 SYBR Green qPCR Mastermix (Qiagen 330502, Hilden, Germany) before loading onto the sample plate. The sample plate was processed using the QuantStudio3 System (Applied Biosystems, Inc., Waltham, MA, USA) starting with a 10-min incubation at 95 °C, followed by 40 cycles of denaturation at 95 °C for 15 s and annealing/extension at 60 °C for 30 s. Geneglobe (Qiagen, Hilden, Germany) was used for comparison studies, fold change regulation, and heatmap generation. The detection threshold was standardized to 20,000. The CT threshold is set to 35, and control genes were normalized using geometric means.

2.8.4. Gene Ontology Analysis

A gene ontology (GO) analysis was performed based on the heatmaps generated from RT-qPCR data. Differentially expressed genes were quantified using log₂-fold change and reported as up- or downregulated, relative to a CDM control. Groups compared CDM vs. CDM, both without H₂O₂, and CDM vs. D10S, both with H₂O₂ and DFO treatment. GO enrichment analysis was performed using the PANTHER Classification System (v19.0, <https://pantherdb.org/> (accessed on 17 December 2024)). The individual genes were entered into the database, specifying *Rattus norvegicus* as the reference species. Functional annotation categories included biological process, molecular function, cellular component, and protein classification. Due to biological replicates of n = 1 per condition, statistical testing for the RT-qPCR results was not conducted.

3. Results

3.1. Variation in SC Morphology Between Serum-Containing and Serum-Free Conditions

Schwann cell morphology varied between serum-containing and serum-free conditions, with distinct differences observed in soma and cellular processes. In serum-containing conditions, SCs exhibited a more expanded soma, which appeared flatter and covered a larger surface area (Figure 1B). In contrast, SCs cultured in serum-free conditions displayed a more compact, needle-like bipolar soma characterized by a narrower and more defined structure (Figure 1C). Similarly, differences were observed in the morphology of SC processes. In serum-containing conditions, SC processes were comparatively shorter

and remained proximal to the soma with limited extension (Figure 1B). In contrast, SCs in serum-free conditions displayed more extended, fiber-like processes that stretched distally and formed bipolar processes from the soma, indicative of a more differentiated state (Figure 1C). SCs in serum-containing and serum-free conditions also responded differently in the event of H₂O₂-induced oxidative stress. In serum-containing conditions, SC morphology and density were greatly altered in the presence of H₂O₂-challenge (Figure 1B), whereas a more consistent SC phenotype was observed in serum-free conditions (Figure 1C).

3.2. Growth Factors Failed to Promote SC Survival Following H₂O₂ Exposure

We investigated the potential of growth factors to enhance cellular survival following H₂O₂-induced oxidative stress. By following the experimental paradigm (Figure 2A), SCs were pre-treated with either fibroblast growth factor 2 (FGF2), fibroblast growth factor 5 (FGF5), or Neuregulin Beta1 (NRG)—in D10S Mit media (Supplementary Table S2) for 24 h prior to H₂O₂ exposure. Following their pretreatments, SCs were analyzed by immunofluorescence staining to evaluate DAPI, p75, and GFAP expression (Figure 2C). SC survival was evaluated by quantifying GFAP-positive SC nuclei, followed by statistical analysis. Comparing growth factors pretreated SCs without H₂O₂ control, D10S Mit, shows significantly increased proliferation (Figure 2B; D10S + Mit vs. D10S + Mit + FGF2, $p = 7.26 \times 10^{-22}$, ****; D10S + Mit vs. D10S + Mit + FGF5, $p = 3.19 \times 10^{-4}$, ***; D10S + Mit vs. D10S + 3F, $p = 4.76 \times 10^{-7}$, ****), validating their role in promoting proliferation of SCs. However, SCs were not protected against H₂O₂-induced cell death when pre-treated with growth factors, as differences in GFAP-positive SC nuclei across treatments were statistically insignificant (Figure 2B), indicating that pretreatment with growth factors is not sufficient to protect SCs against reactive oxygen species-induced cell death (D10S + Mit control vs. D10S + Mit + H₂O₂, $p = 1.51 \times 10^{-2}$, *; D10S + Mit + FGF2 control vs. D10S + Mit + FGF2 + H₂O₂, $p = 7.26 \times 10^{-22}$, ****; D10S + Mit + FGF5 control vs. D10S + Mit + FGF5 + H₂O₂, $p = 1.63 \times 10^{-9}$, ****; D10S + 3F control vs. D10S + 3F + H₂O₂, $p = 1.09 \times 10^{-10}$, ****). Morphological observations from confocal images of SCs grown in selected growth factors (Figure 2C) confirmed that growth factors promoted the typical elongated morphology of in vitro cultured SCs.

3.3. Deferoxamine Mesylate (DFO) Increased SC Survival Following H₂O₂ Challenge in Serum-Containing Conditions

Deferoxamine mesylate (DFO) is an FDA-approved iron chelator previously suggested to enhance Schwann cell survival in hypoxic conditions [22]. We tested if DFO could effectively prevent H₂O₂-induced SC death in serum-containing conditions (D10S). We also tested whether the addition of 3F during DFO treatment would influence DFO's protective effect against H₂O₂-induced oxidative stress. We hypothesized that 3F would prime SCs for growth and proliferation, which could, in turn, impair their ability to respond to H₂O₂ induced cell death. Following their treatment protocols (Figures 3A and 4A), SC survival was evaluated by quantifying GFAP-positive SC nuclei, followed by statistical analysis via Tukey's HSD test. Results showed that, under H₂O₂-induced cell death, SC did not survive in D10S (Figure 3B; D10S + H₂O₂ vs. D10S -H₂O₂, $p = 1.15 \times 10^{-13}$, ****). Additionally, inclusion of 3F did not lead to any significant improvement in SC survival (Figure 3B; D10S + 3F + H₂O₂ vs. D10S + 3F control, $p = 3.73 \times 10^{-14}$, ****), consistent with our previous findings that 3F does not provide any protective effect against oxidative stress (Figure 2B; D10S 3F + H₂O₂ vs. D10S 3F control, $p = 1.09 \times 10^{-10}$, ****). We added DFO to evaluate its effects on SC survival and phenotype in the presence of H₂O₂-induced cell death. The inclusion of DFO in both D10S and D10S 3F medium protected SCs and increased survival following exposure to H₂O₂ (Figure 3B; D10S + H₂O₂ vs. D10S + DFO + H₂O₂, $p = 2.39 \times 10^{-10}$, ****; D10S 3F + H₂O₂ vs. D10S 3F + DFO + H₂O₂, $p = 1.18 \times 10^{-13}$,

****). Furthermore, comparisons between D10S DFO + H₂O₂ and D10S -H₂O₂ showed no significant difference in SC survival, indicating that DFO reduced H₂O₂-induced cell death and restored SC survival to baseline levels. However, in D10S 3F medium, DFO pre-treatment (D10S 3F + DFO +H₂O₂) did not protect SC survival to baseline levels (D10S -H₂O₂). This suggests that while 3F is essential in promoting SC proliferation, it can interfere with the effects of DFO and reduce its protectiveness. Nonetheless, these results showed that DFO conferred significant protection against H₂O₂-induced cell death in serum-containing conditions. Immunofluorescent staining indicated that H₂O₂ challenge resulted in altered SC morphology and non-uniform SC distribution in serum-containing conditions (Figure 3C).

3.4. Serum-Free Media Protected SCs Against H₂O₂-Induced Cell Death Without DFO

We also investigated if DFO could effectively prevent H₂O₂-induced cell death in serum-free medium: CDM, which is a DMEM/F12 medium supplemented with bovine insulin, human transferrin, sodium selenite, and putrescine (Supplementary Table S1). The experimental protocol and quantification methods outlined in Section 3.3 were repeated with the only modification being the substitution of serum-containing D10S with serum-free CDM as the base medium (Figure 4A). Interestingly, CDM alone was sufficient to promote SC survival under H₂O₂-induced cell death (Figure 4B, CDM -H₂O₂ vs. CDM +H₂O₂, $p = 1.157 \times 10^{-13}$, ns). Even without the addition of DFO, CDM alone restored SC survival to baseline levels, suggesting that factors in CDM may contribute to preventing H₂O₂-induced cell death. Here, the inclusion of 3F did not decrease the protection provided by CDM against H₂O₂ induced cell death (Figure 4B, CDM 3F -H₂O₂ vs. CDM 3F +H₂O₂, $p = 5.037 \times 10^{-2}$, ns), indicating that 3F is not sufficient to interfere with the effects of CDM and reduce its protectiveness, unlike their serum counterpart. The inclusion of DFO in serum-free CDM did not affect SC survival in H₂O₂-induced cell death, indicating that DFO is unnecessary in serum-free CDM to promote SC survival (Figure 4B, CDM DFO -H₂O₂ vs. CDM DFO +H₂O₂, $p = 9.989 \times 10^{-1}$, ns). Immunofluorescent staining showed SC distribution and morphology was mostly unaffected after H₂O₂-challenge in serum-free conditions (Figure 4C).

3.5. Hif1 α Expression Consistent in Serum-Free Conditions but Inconsistent in Serum Conditions

It is previously reported that DFO acts as a neuroprotective agent through the upregulation of the hypoxia-inducible factor (HIF) protein family to promote cellular survival in hypoxic environments such as the ROS-rich environment in our study. We tested if Hif1 α will be upregulated here with our SCs. To this end, we have stained for hypoxia-inducible factor 1 alpha (Hif1 α) and subsequently quantified the protein expression using whole cell corrected total cell fluorescence (WC-CTCF). Statistical analysis of the Hif1 α WC-CTCF reveals a consistent Hif1 α expression across serum-free groups regardless of DFO pretreatment or H₂O₂ challenge (Figure 5B). Hif1 α expression in serum shows variable expression with a significantly high expression of Hif1 α in D10S (Figure 5B, D10S -H₂O₂ vs. D10S +H₂O₂, $p = 1.800 \times 10^{-2}$, *) and D10S 3F (Figure 5B, $p = 2.300 \times 10^{-4}$, ***) without H₂O₂ challenge (Figure 5B). Qualitative analysis on immunocytochemistry images reveals localized nuclear expression of Hif1 α in serum-free conditions and higher levels of cytoplasmic Hif1 α expression in non-DFO pretreated and non-H₂O₂ challenged SCs in serum conditions (Figure 5C).

3.6. Serum Drives High Variability in Collagen IV Expression

The secretion profile of the extracellular matrix (ECM) by SCs plays a critical role in SC adhesion, maturation, and subsequent nerve regeneration following transplantation. Collagen IV is one of the key ECM elements expressed by SCs involved in the regeneration

of myelin sheath, an indicator of SC maturation [35]. Wei investigated whether the addition of DFO would influence the collagen IV expression profile of SCs under both serum and serum-free conditions, with and without H₂O₂-induced cell death. Collagen IV expression was analyzed through immunofluorescence staining, followed by WC-CTCF analysis to quantify collagen IV expression (Section 2.7). WC-CTCF analyses revealed varying patterns of collagen IV expression between SCs in serum-containing and serum-free medium. Collagen IV expression was generally consistent across SCs cultured in CDM. The addition of DFO did not result in any measurable changes in collagen IV expression in the majority of CDM groups when compared to their non-DFO treated counterparts (statistics shown in Supplementary Table S6), suggesting that DFO did not alter the ECM expression of collagen IV in serum-free conditions. Surprisingly, when SCs are challenged with H₂O₂ in CDM medium (CDM + H₂O₂), collagen IV expression shows a significant drop compared to control (CDM -H₂O₂), indicating that DFO or 3F may be needed in serum-free conditions to promote the production of extracellular collagen IV in SCs in the presence of ROS. In serum conditions, collagen IV expression is highly variable. When pretreating SCs with 3F, collagen IV expression is highly upregulated without the presence of ROS (Figure 6; D10S 3F -H₂O₂ vs. D10S 3F +H₂O₂, $p = 1.000 \times 10^{-5}$, ****). However, when pretreatment includes DFO, the upregulation of collagen IV is diminished. Overall, SCs in serum conditions exhibit largely variable collagen IV expression compared to serum-free conditions.

3.7. Serum vs. Serum-Free Conditions Show Differential Transcriptional Responses in Cell Death Pathways

We asked if treatment with DFO leads to transcriptional changes in cell death pathways, specifically apoptosis, necrosis, and autophagy pathways. To this end, we have isolated RNA from SCs in varying conditions (Supplementary Table S8) for use in RT-qPCR to investigate transcriptional changes in cell death pathways. The fold changes of genes were measured as upregulation or downregulation in serum-free (CDM) groups relative to serum-containing (D10S) groups. The largest fold changes when comparing CDM vs. D10S without H₂O₂ were observed in genes associated with necrosis, specifically downregulation of *Maco1* (−220.02) and *Mag* (−24.68). The largest fold change observed in this group was for *Olr1583* (20.47), which plays a key role in necrosis. In comparison, DFO and H₂O₂-treated groups (CDM + DFO + H₂O₂ vs. D10S + DFO + H₂O₂) showed the greatest fold changes in both anti-apoptotic genes and necrosis genes. The largest upregulation was seen in genes associated with necrosis, including *Defb1* (21.09) and *Hspbp1* (11.68). In contrast, the top downregulated genes were *Tnfrsf11b* (−17.64) and *Bcl2L11* (−8.08), both of which are associated with anti-apoptotic pathways. Considering the substantial reduction of *Maco1* transcription when comparing CDM vs. D10S, genes associated with autophagy, *Ins2* (19.87) and *Esr1* (17.1), showed the next largest increase in transcription. Overall, the data suggest CDM primarily reduces genes involved in necrosis while increasing genes associated with autophagy in the absence of H₂O₂. When both groups are treated with DFO and H₂O₂, genes involved in necrosis are upregulated, while anti-apoptotic transcripts are suppressed. Interestingly, fold changes for autophagy genes appear largely unchanged. Heatmaps of RT-qPCR are shown in Figures 7 and 8.

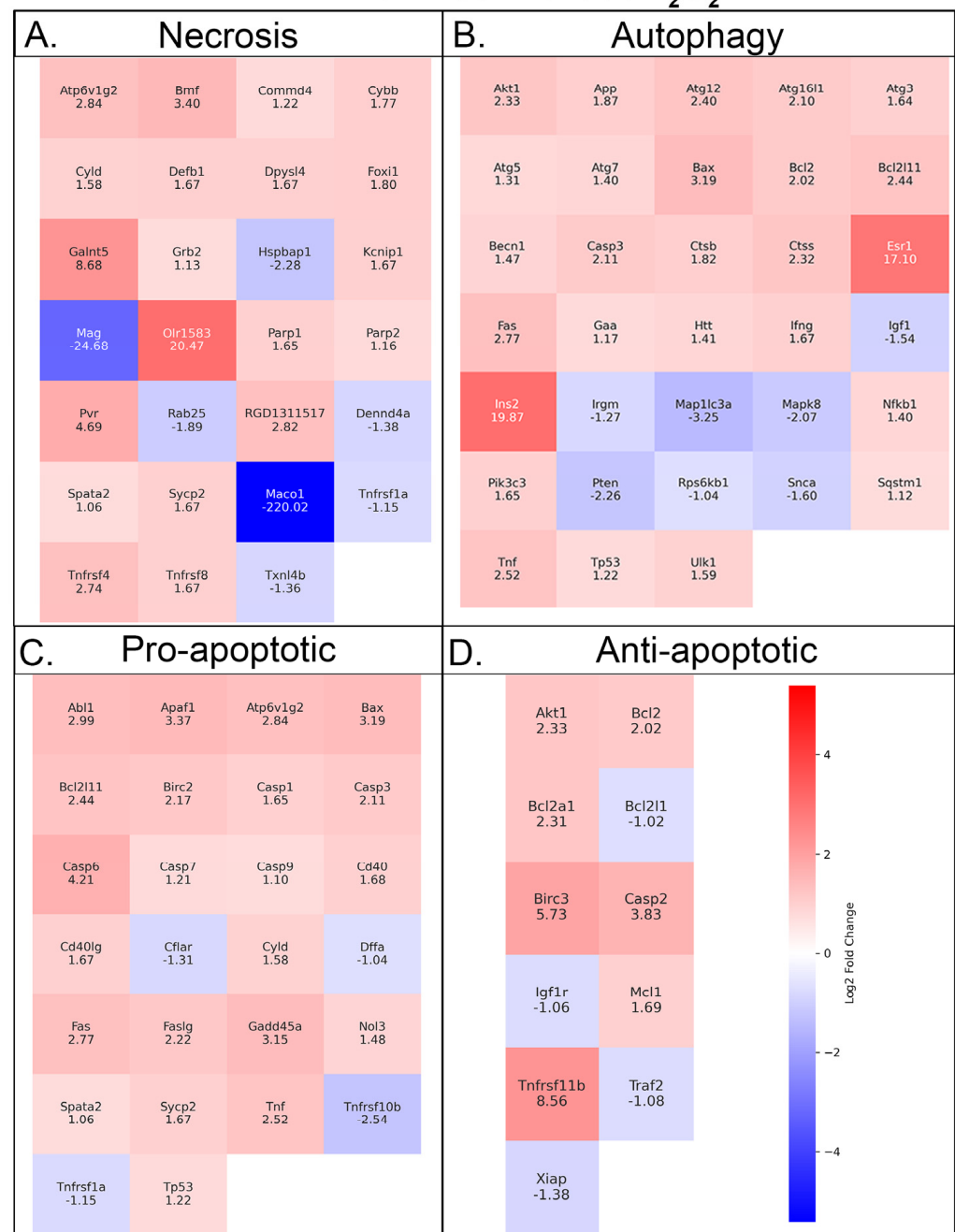
CDM vs D10s without H₂O₂

Figure 7. RT-qPCR shows increased metabolism and autophagy in CDM medium. Heatmaps showing Schwann cells in serum-free versus serum medium without the presence of H₂O₂, and transcript expression associated with (A) necrosis, (B) autophagy, (C) pro-apoptotic, and (D) antiapoptotic pathways. Fold-change values are shown on the heatmap.

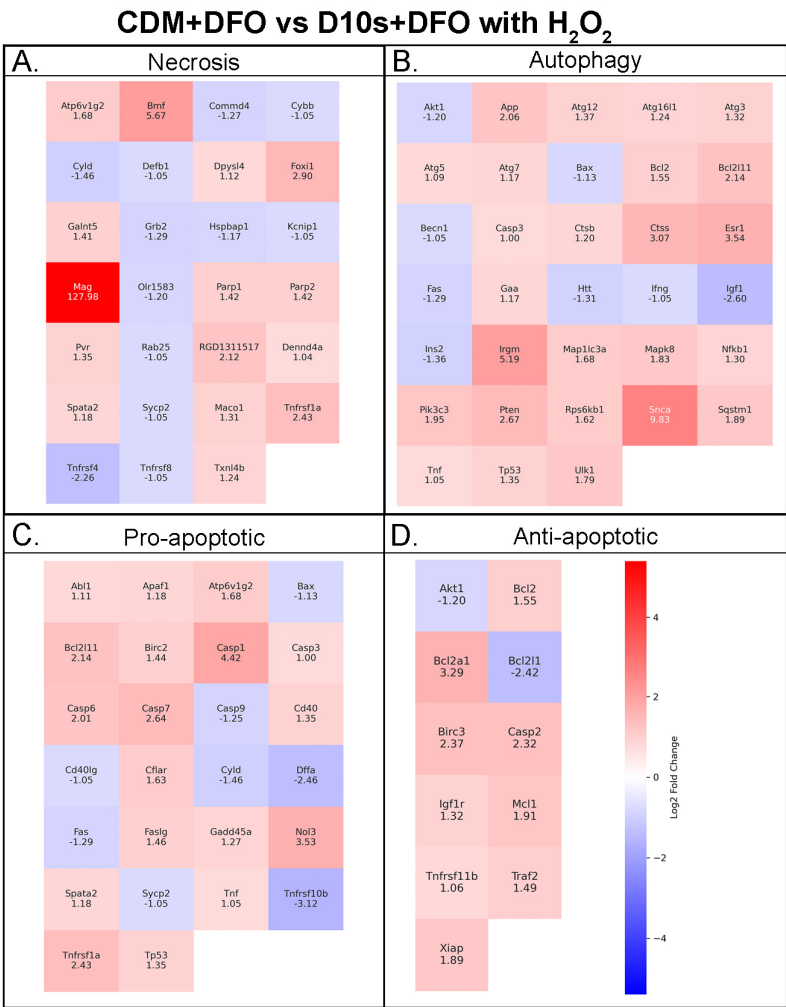


Figure 8. RT-qPCR shows pro-repair and pro-regenerative Schwann cells in CDM media in the presence of DFO and H₂O₂. Heatmaps showing Schwann cells in serum-free versus serum medium with the presence of DFO and H₂O₂, and transcript expression associated with (A) necrosis, (B) autophagy, (C) pro-apoptotic, and (D) antiapoptotic pathways. Fold-change values are shown on the heatmap.

4. Discussion

We examined the effect of deferoxamine mesylate (DFO) on the survival of ventral root Schwann cells isolated from adult Sprague Dawley rats in H₂O₂-induced cell death. It was previously reported that DFO increases SC survival in H₂O₂-induced cell death and hypoxic conditions in vitro in serum-containing conditions [23,39]. Here, we expanded the horizon to study DFO’s effectiveness in protecting SCs from H₂O₂-induced cell death in more clinically relevant, serum-free conditions and presented our results through phenotypic staining, SC survival quantification, whole cell corrected total cell fluorescence (WC-CTCF) analysis, and RT-qPCR cell death transcriptomics analysis.

4.1. Distinctive SC Morphology in Serum and Serum-Free Conditions

Consistent with previous findings from Plant and colleagues [30,39], SCs exhibited drastically different morphology between serum-containing and serum-free conditions (Figure 1). The differential morphology of the two culture conditions affects SC maturation and regenerative capacity in vivo. For instance, the bipolar and spindle morphology of SCs in CDM shows a pro-regenerative phenotype in comparison to the small and flat phenotype of SCs in D10S. The spindle morphology allows for neurites to grow on top, acting as a bridging mechanism and allowing for nerve regeneration. However, SCs in

serum conditions switch from a regenerative state into a proliferative state and abandon cell contact [40]. Thus, SCs grown in serum appear to be more prone to H_2O_2 -induced cell death due to the energetic switch to a proliferative state. Furthermore, serum has been reported to lead to unstable and variable phenotypes in vitro in mesenchymal stromal cells and olfactory ensheathing glia [41–43]. Although the literature lacks work describing SCs in serum versus serum-free medium, the use of serum would still largely decrease the reproductive capacity of SC cultures in transplantation studies due to the lot-to-lot variability in serum production.

4.2. Growth Factors Provide No Protection Against H_2O_2 -Induced Cell Death

We asked if growth factors would be able to attenuate H_2O_2 -induced cell death in Schwann cells (SCs). We pre-treated SCs with fibroblast growth factor 2 (FGF2), or fibroblast growth factor 5 (FGF5), or neuregulin beta 1 (NRGb1), for 24 h prior to 16 h of 62.5 mM H_2O_2 challenge. Our results indicate no survival of SCs following H_2O_2 challenge regardless of pretreatment. Although it has been previously reported that these factors attenuate H_2O_2 -induced cell death in alternative cell types such as embryonic cortical neurons [44] and bone marrow mesenchymal stem cells [45], we have shown that they do not attenuate H_2O_2 cell death in adult SCs. Here, we did not test these growth factors independently in serum-free conditions. In serum-free conditions, growth factors could produce a stronger protectiveness in addition to the serum-free protectiveness through the promotion of proliferation. However, as seen with SCs grown in 3F, it may also drive SCs into growth states and thus reduce their capacity to withstand H_2O_2 -induced cell death.

4.3. DFO Efficacy in Serum and Serum-Free Conditions

Here, we have shown that serum-free CDM medium seems to protect SCs from H_2O_2 -induced cell death regardless of DFO pre-treatment. In serum conditions, Hill and colleagues [22,26] have previously established DFO effectiveness in vitro, showing its ability to upregulate Hif1 α and increase cellular survival by means of live–dead staining [22]. However, we have shown here that the use of CDM without DFO pretreatment was able to achieve similar levels of protection against H_2O_2 cell death to DFO in serum-containing D10S medium. The use of CDM is also shown to be a better alternative due to its consistency that is largely unachievable in serum-based treatments due to high variation in serum, which contains variable and trace amounts of growth factors such as BDNF, FGF5, FGF2, and NRG beta 1, which vary from batch to batch in serum production [46]. While DFO has been proven to increase SC survival in serum-containing conditions [22], most of its effects are masked by the inherent protectiveness provided in CDM, suggesting that the inclusion of DFO in CDM may not be necessary to achieve H_2O_2 -induced cell death protection.

4.4. Transferrin in CDM Medium May Influence HiF-PhD to Override DFO Effects in SCs

The combined factors of transferrin, insulin, and sodium selenite, also known as ITS serum-free supplement, are a long-established serum-free alternative to the use of fetal bovine serum supplement in tissue culture medium. These factors are critical in supporting cellular proliferation, survival, and glucose uptake. Specifically, transferrin acts as an iron transporter and has been reported to decrease iron accumulation in Parkinson's disease-affected neurons [47]. Mechanistically, transferrin receptor (TfR) acts downstream of Hif1 α expression, allowing cells to uptake higher levels of iron during low oxygen environments for increased mitochondrial activity [48,49]. With the addition of transferrin in the serum-free medium, the process of Hif1 α modulated upregulation of TfR may be overwritten by the presence of transferrin to sufficiently provide iron to SCs and may shut down DFO-facilitated HiF-PhD inhibition with increased iron levels, leading to our observed levels of SC Hif1 α expression in serum-free conditions (Figure 5C). It may be of

interest to pursue the individual effects of each supplement component in H₂O₂-induced SC death to further characterize the protection offered in CDM.

4.5. Nuclear Expression of Hif1 α Facilitates Protection in Serum-Free Cultured or DFO Pre-Treated SCs

We have quantitated whole cell Hif1 α expression via WC-CTCF. Here, we see a consistent nuclear expression of Hif1 α in SCs grown in serum-free conditions (Figure 5B,C) but with an inconsistent expression of Hif1 α in SCs grown in serum conditions (Figure 5B). Furthermore, ICC reveals a cytoplasmic expression of Hif1 α in non-H₂O₂ challenged SCs in serum conditions (D10S -H₂O₂ and D10S 3F -H₂O₂, Figure 5C). Previous work has reported the expression of Hif1 α enhances SC survival when transplanted into the spinal cord [47]. Stabilization and subsequent nuclear translocation of Hif1 α allows for binding with hypoxia-response element (HRE) genes and induces protection against oxidative stress through the upregulation of critical angiogenic and protective genes such as vascular endothelial growth factor, or VEGF [50–52], which has previously been reported to be upregulated through western blot and qPCR analysis [22]. Here, our data add strong evidence for this protection such that the DFO pre-treated SCs survived compared to non-DFO pretreated SCs in serum conditions. However, in serum-free conditions, this protectiveness seems to be mediated by an alternative mechanism since, regardless of DFO pretreatment, SCs survived the H₂O₂ challenge. Further, the nuclear expression of Hif1 α seems to be present in SCs in serum-free conditions but further enhanced by the presence of DFO. It may be crucial to determine the mechanism of this protection to understand the protection of SCs against H₂O₂-induced cell death in serum-free conditions. It would be of interest to explore the differences of Hif1 α presence in the cytoplasm and nucleus in serum versus serum-free conditions as well.

4.6. Collagen IV Expression Reveals Proliferative SCs in Serum Media and Pro-Regenerative SCs in Serum-Free Media

We quantitated whole cell fluorescence of collagen IV in SCs to determine if there are any extracellular matrix changes. Collagen IV is an important factor in determining states of SCs; it serves as an indicator of the proliferation and remyelination potential of SCs. We have shown here that by inducing proliferative states in SCs via the addition of the 3F (forskolin, bovine pituitary extract, and neuregulin) in serum-containing medium, survival in H₂O₂-induced cell death is negatively affected such that survival is decreased compared to SCs without proliferative 3F signaling in serum conditions (Figure 4B, D10S 3F -H₂O₂ vs. D10S 3F +H₂O₂, $p = 3.730 \times 10^{-14}$). Subsequent collagen IV quantitation also reveals a higher proliferative state in the D10S + 3F medium condition through a high collagen IV expression when not challenged with H₂O₂, where the proliferative state is shut down following the H₂O₂ challenge (Figure 6, D10S 3F -H₂O₂ vs. D10S 3F +H₂O₂, ****, $p = 1.000 \times 10^{-5}$). Previous work has shown immature or proliferative Schwann cells do not facilitate regeneration as efficiently as matured Schwann cells [26]; our results thus indicate that the more mature states of Schwann cells in serum-free media will facilitate higher regeneration as a cellular transplant, owing to the more stabilized extracellular matrix (Figure 6) and their bipolar process phenotype, which allows for host neurons to bridge the lesion gap (Figures 2 and 4).

4.7. Serum-Free, Chemically Defined Media Shifts SCs Towards Heightened Metabolism and Cellular Recycling Phenotype Without the Presence of H₂O₂ and DFO

Here, we identified numerous differentially expressed genes in our in vitro model of hydrogen peroxide-induced cell death. Transcriptomic changes associated with necrosis, autophagy, and apoptosis were observed, and the GO enrichment analysis has provided

key insights into how these genes affect cell death pathways. In the absence of DFO or H₂O₂, the serum-free group, CDM-H₂O₂, primarily showed changes in genes of the necrotic pathway, especially downregulation of *Maco1* and *Mag*. In addition to the necrosis pathway, these genes play a role in cytoskeletal dynamics, cell adhesion, myelination, and metabolic shifts in response to environmental cues [47]. Given their combined and robust downregulation, these data suggest that the SCs may be undergoing a metabolic shift, allocating cellular resources for energy production and autophagy rather than myelin maintenance or proliferation [53,54]. Within the same treatment group, *OLR1583*, *Ins2*, and *Esr1* were strongly upregulated, which are involved in the necrosis and autophagy pathways [54]. Although supplementary roles of these genes support the inference that the SCs are indeed shifting toward a pro-survival phenotype. Aside from smell, olfactory receptors can aid in modulating intracellular signaling in response to a dynamic extracellular environment [55,56]. In addition, they can influence myelin maintenance pathways, which rely on lipid synthesis and degradation. Acting as an extracellular sensor, *Olr1583* may facilitate metabolic adaptations and reallocation required for myelin recycling and maintenance [57,58]. Furthermore, *Ins2* and *Esr1* have been found to have supporting roles in these processes. Upregulation of the *Ins2* gene suggests an increased activation of insulin signaling pathways, such as the MAPK/ERK cascade. These pathways are known to promote autophagy and survival under cellular stress [59]. In an accompanying role, it is well established that increases in estrogen-related pathways play critical roles in cellular homeostasis, particularly supporting autophagy [60,61]. Taken together, the combined downregulation of *Maco1* and *Mag*, along with the upregulation of *Olr1583*, *Ins2*, and *Esr1*, supports the consensus that serum-free media in the absence of H₂O₂ increases transcription of genes associated with a phenotypic and metabolic shift toward autophagy or cellular stress when compared to serum-containing media. Alternatively, the increased survival phenotype could be induced by serum starvation, which has historically shifted SCs into a survival state [62]. This pro-survival state has been shown to be reversible upon re-exposure to serum.

4.8. Chemically Defined Media Facilitates Pro-Regenerative States and Cell Metabolism in the Presence of Deferoxamine Mesylate and 62.5 mM H₂O₂

When both serum-free CDM and serum-containing media, D10S, were treated with DFO in the presence of 62.5 mM H₂O₂, the transcriptional landscape was largely changed (Figure 8). The most prominent fold changes were observed in *Defb1* (21.09) and *Tnfrsf11b* (−17.64). Beta defensins, such as *Defb1*, are known to directly participate in redox-dependent mechanisms. Their reduced form improves anti-microbial function [63]. In SCs, increased ROS levels could induce *Defb1* expression to mitigate oxidative stress. The observed upregulation suggests an active oxidative stress management response, which can result from increased ROS production during high metabolic activity or in the presence of H₂O₂ [64]. Conventionally, an increase in oxidative stress would concurrently show a rise in *Tnfrsf11b* expression. This upregulation can act as a “gauge” of cellular stress, as elevated *Tnfrsf11b* exacerbates ROS production by mitochondria [65]. If oxidative damage begins to overwhelm these compensatory mechanisms, *Tnfrsf11b* expression would further increase, ultimately shifting the SC from autophagy toward an apoptotic phenotype [66]. Combined, both the upregulation of *Defb1* and downregulation of *Tnfrsf11b* suggest the SCs are actively managing oxidative stress, carefully balancing autophagy and apoptosis. Supporting evidence includes the suppression of *Bcl2l11* and *Bcl112*, which is consistent with the assumption that the SCs are indeed successfully regulating oxidative stress [59,67,68]. Additionally, changes in *Hspbap1* (11.68), *Sycp2* (7.45), *Ins2* (6.5), *Birc3* (−5.42), and *Htt* (4.64) further indicate a pro-autophagy phenotype, favoring intracellular stability [69–72]. Notably, *Ins2* upregulation suggests an adaptation needed to meet the

increased energy demands of these metabolic changes [73], while upregulation of *Htt* indicates a persisting myelinating phenotype [74]. Overall, the observed transcriptional changes when comparing serum-free vs. serum-containing media indicate that the former promotes autophagy and cellular recycling at greater levels when in the presence of 62.5 mM H₂O₂ and DFO. This adaptation permits the continued repair and maintenance required for SCs to retain their pro-repair and regenerative phenotypes in the more hostile microenvironment of injury.

5. Conclusions

We have investigated the efficacy of deferoxamine mesylate (DFO) in protecting ventral root Schwann cells (SCs) isolated from adult Sprague Dawley rats from H₂O₂-induced cell death. Our results show that pre-treatment using DFO increases SCs survival in serum conditions but has no effect in serum-free conditions, which is not consistent with our hypothesis. Instead, in serum-free conditions, SCs survive H₂O₂-induced cell death regardless of being pre-treated with DFO. Our analysis of SC phenotype and transcriptomics reveals a pro-repair and pro-survival state of SCs in serum-free conditions. In serum, DFO maintained efficacy in preventing cell death. Per our hypothesis, SCs were expected to have an increased survival upon DFO pretreatment; our results have shown that it is only the case when SCs are grown in serum-containing conditions. Without serum, SCs innately turn into a pro-survival state.

Previously, studies on DFO on increasing SC survival have been performed in serum-containing conditions; our results show a more pro-survival state of SCs in serum-free media, making DFO seemingly unnecessary. Thus, our findings highlight the importance of media differences and the need to replicate clinically used, serum-free media in *in vitro* and *in vivo* studies to accurately reflect SC physiology when treated with factors.

Translationally, we have shown that DFO is not worthy of further investigation since it fails to increase cellular survival in serum-free mediums. However, it emphasized the importance of studying the effects of similar pharmaceutical agents in serum-free conditions to accurately reflect clinical practice. Future studies must consider the effects of serum in modifying Schwann cell phenotypes when conducting a similar study. Additionally, it may be of interest for future studies to ascertain the molecular mechanisms of how the use of serum-free medium or serum starvation shifts SCs into a pro-survival state and thus increases SC survival *in vivo*.

Supplementary Materials: The following supporting information can be downloaded at: <https://www.mdpi.com/article/10.3390/cells14060461/s1>, Table S1. Media components; Table S2. Pre-treatment groups for survival quantification (Figures 2–4); Table S3. Pretreatment groups for WC-CTCF (Hif1 α); Table S4. Pretreatment groups for WC-CTCF (Collagen IV); Table S5. Pretreatment groups for RT-qPCR (Figures 7 and 8); Table S6. Gene list and associated pathways for RT-qPCR; Table S7. p values for cell survival counts in serum groups; Table S8. p values for SC survival counts in serum-free groups; Table S9. p values for Hif1 α WC-CTCF; Table S10: p values for Collagen IV WC-CTCF.

Author Contributions: Conceptualization, Y.H.E.M., A.R.P. and G.W.P.; methodology, Y.H.E.M. and G.W.P.; software, S.R.V., C.H.H.C. and A.R.P.; validation, Y.H.E.M.; formal analysis, C.H.H.C. and S.R.V.; investigation, Y.H.E.M. and A.R.P.; resources, P.M. and G.W.P.; data curation, Y.H.E.M., C.H.H.C. and S.R.V.; writing—original draft preparation, Y.H.E.M.; writing—review and editing, Y.H.E.M., S.R.V., C.H.H.C., P.M. and G.W.P.; visualization, Y.H.E.M., S.R.V., A.R.P., C.H.H.C. and G.W.P.; supervision, Y.H.E.M. and G.W.P.; project administration, Y.H.E.M. and G.W.P.; funding acquisition, G.W.P. All authors have read and agreed to the published version of the manuscript.

Funding: This research was funded by Ohio State University, grant number 125100.

Institutional Review Board Statement: The animal study was approved by the IACUC with approval code 2023A00000084 on the 9th of January in 2024.

Informed Consent Statement: Not applicable.

Data Availability Statement: The raw data supporting the conclusions of this article will be made available by the authors on request.

Acknowledgments: Research reported in this publication was supported by The Ohio State University Comprehensive Cancer Center and the National Institutes of Health under grant number P30 CA016058. We thank the Genomics Core Shared Resource at The Ohio State University Comprehensive Cancer Center, Columbus, OH, for RNA purification and integrity validation.

Conflicts of Interest: The authors declare no conflicts of interest.

References

1. Bennett, J.; Das, J.M.; Emmady, P.D. Spinal Cord Injuries. In *StatPearls [Internet]*; StatPearls Publishing: Treasure Island, FL, USA, 2024. Available online: <https://www.ncbi.nlm.nih.gov/books/NBK560721/> (accessed on 23 August 2024).
2. O'Shea, T.M.; Burda, J.E.; Sofroniew, M.V. Cell biology of spinal cord injury and repair. *J. Clin. Investig.* **2017**, *127*, 3259–3270. [CrossRef]
3. Tran, A.P.; Warren, P.M.; Silver, J. The Biology of Regeneration Failure and Success After Spinal Cord Injury. *Physiol. Rev.* **2018**, *98*, 881–917. [CrossRef] [PubMed]
4. Hill, C.E. A view from the ending: Axonal dieback and regeneration following SCI. *Neurosci. Lett.* **2017**, *652*, 11–24. [CrossRef] [PubMed]
5. Bunge, M.B.; Pearse, D.D. Transplantation strategies to promote repair of the injured spinal cord. *J. Rehabil. Res. Dev.* **2003**, *40* (Suppl. 1), 55–62. [CrossRef] [PubMed]
6. Assinck, P.; Duncan, G.J.; Hilton, B.J.; Plemel, J.R.; Tetzlaff, W. Cell transplantation therapy for spinal cord injury. *Nat. Neurosci.* **2017**, *20*, 637–647. [CrossRef]
7. Ribeiro, B.F.; da Cruz, B.C.; de Sousa, B.M.; Correia, P.D.; David, N.; Rocha, C.; Almeida, R.D.; Ribeiro da Cunha, M.; Marques Baptista, A.A.; Vieira, S.I. Cell therapies for spinal cord injury: A review of the clinical trials and cell-type therapeutic potential. *Brain* **2023**, *146*, 2672–2693, Erratum in *Brain* **2023**, *146*, e128. <https://doi.org/10.1093/brain/awad204>. [CrossRef]
8. Deng, L.X.; Walker, C.; Xu, X.M. Schwann cell transplantation and descending propriospinal regeneration after spinal cord injury. *Brain Res.* **2015**, *1619*, 104–114. [CrossRef] [PubMed] [PubMed Central]
9. Barbour, H.R.; Plant, C.D.; Harvey, A.R.; Plant, G.W. Tissue sparing, behavioral recovery, supraspinal axonal sparing/regeneration following sub-acute glial transplantation in a model of spinal cord contusion. *BMC Neurosci.* **2013**, *14*, 106. [CrossRef]
10. Marquardt, L.M.; Douglames, V.M.; Wang, A.T.; Dubbin, K.; Suhar, R.A.; Kratochvil, M.J.; Medress, Z.A.; Plant, G.W.; Heilshorn, S.C. Designer, injectable gels to prevent transplanted Schwann cell loss during spinal cord injury therapy. *Sci. Adv.* **2020**, *6*, eaaz1039. [CrossRef] [PubMed] [PubMed Central]
11. Anderson, K.D.; Guest, J.D.; Dietrich, W.D.; Bartlett Bunge, M.; Curiel, R.; Dididze, M.; Green, B.A.; Khan, A.; Pearse, D.D.; Saraf-Lavi, E.; et al. Safety of Autologous Human Schwann Cell Transplantation in Subacute Thoracic Spinal Cord Injury. *J. Neurotrauma* **2017**, *34*, 2950–2963. [CrossRef]
12. Bunge, M.B.; Monje, P.V.; Khan, A.; Wood, P.M. From transplanting Schwann cells in experimental rat spinal cord injury to their transplantation into human injured spinal cord in clinical trials. *Prog. Brain Res.* **2017**, *231*, 107–133. [CrossRef] [PubMed]
13. Guest, J.; Santamaria, A.J.; Benavides, F.D. Clinical translation of autologous Schwann cell transplantation for the treatment of spinal cord injury. *Curr. Opin. Organ. Transplant.* **2013**, *18*, 682–689. [CrossRef] [PubMed] [PubMed Central]
14. David, S.; Aguayo, A.J. Axonal elongation into peripheral nervous system “bridges” after central nervous system injury in adult rats. *Science* **1981**, *214*, 931–933. [CrossRef]
15. Ceto, S.; Sekiguchi, K.J.; Takashima, Y.; Nimmerjahn, A.; Tuszynski, M.H. Neural Stem Cell Grafts Form Extensive Synaptic Networks that Integrate with Host Circuits after Spinal Cord Injury. *Cell Stem Cell* **2020**, *27*, 430–440.e5. [CrossRef] [PubMed]
16. Dulin, J.N.; Lu, P. Bridging the injured spinal cord with neural stem cells. *Neural Regen. Res.* **2014**, *9*, 229–231. [CrossRef]
17. Swijnenburg, R.J.; Schrepfer, S.; Govaert, J.A.; Cao, F.; Ransohoff, K.; Sheikh, A.Y.; Haddad, M.; Connolly, A.J.; Davis, M.M.; Robbins, R.C.; et al. Immunosuppressive therapy mitigates immunological rejection of human embryonic stem cell xenografts. *Proc. Natl. Acad. Sci. USA* **2008**, *105*, 12991–12996. [CrossRef]
18. Steward, O.; Sharp, K.G.; Yee, K.M.; Hatch, M.N.; Bonner, J.F. Characterization of ectopic colonies that form in widespread areas of the nervous system with neural stem cell transplants into the site of a severe spinal cord injury. *J. Neurosci.* **2014**, *34*, 14013–14021. [CrossRef]

19. Yin, Z.; Wan, B.; Gong, G.; Yin, J. ROS: Executioner of regulating cell death in spinal cord injury. *Front. Immunol.* **2024**, *15*, 1330678. [CrossRef] [PubMed] [PubMed Central]
20. Aparicio, G.I.; Monje, P.V. Human Schwann Cells in vitro I. Nerve Tissue Processing, Pre-degeneration, Isolation, and Culturing of Primary Cells. *Bio-Protocol* **2023**, *13*, e4748. [CrossRef]
21. Monje, P.V. Schwann Cell Cultures: Biology, Technology and Therapeutics. *Cells* **2020**, *9*, 1848. [CrossRef]
22. David, B.T.; Curtin, J.J.; Brown, J.L.; Coutts, D.J.C.; Boles, N.C.; Hill, C.E. Treatment with hypoxia-mimetics protects cultured rat Schwann cells against oxidative stress-induced cell death. *Glia* **2021**, *69*, 2215–2234. [CrossRef] [PubMed]
23. Chao, P.Y.; Lin, J.A.; Ye, J.C.; Hwang, J.M.; Ting, W.J.; Huang, C.Y.; Liu, J.Y. Attenuation of Oxidative Stress-Induced Cell Apoptosis in Schwann RSC96 Cells by *Ocimum gratissimum* Aqueous Extract. *Int. J. Med. Sci.* **2017**, *14*, 764–771. [CrossRef]
24. Fideles, S.O.M.; de Cássia Ortiz, A.; Buchaim, D.V.; de Souza Bastos Mazuqueli Pereira, E.; Parreira, M.J.B.M.; de Oliveira Rossi, J.; da Cunha, M.R.; de Souza, A.T.; Soares, W.C.; Buchaim, R.L. Influence of the Neuroprotective Properties of Quercetin on Regeneration and Functional Recovery of the Nervous System. *Antioxidants* **2023**, *12*, 149. [CrossRef] [PubMed]
25. Siriphorn, A.; Chompoonpong, S.; Floyd, C.L. 17 β -estradiol protects Schwann cells against H₂O₂-induced cytotoxicity and increases transplanted Schwann cell survival in a cervical hemicontusion spinal cord injury model. *J. Neurochem.* **2010**, *115*, 864–872. [CrossRef] [PubMed]
26. David, B.T.; Curtin, J.J.; Goldberg, D.C.; Scorpio, K.; Kandaswamy, V.; Hill, C.E. Hypoxia-Inducible Factor 1 α (HIF-1 α) Counteracts the Acute Death of Cells Transplanted into the Injured Spinal Cord. *eNeuro* **2020**, *7*, ENEURO.0092-19.2019. [CrossRef]
27. Singhal, R.; Mitta, S.R.; Das, N.K.; Kerk, S.A.; Sajjakulnukit, P.; Solanki, S.; Andren, A.; Kumar, R.; Olive, K.P.; Banerjee, R.; et al. HIF-2 α activation potentiates oxidative cell death in colorectal cancers by increasing cellular iron. *J. Clin. Investig.* **2021**, *131*, e143691. [CrossRef]
28. Yu, P.; Zhang, G.; Hou, B.; Song, E.; Wen, J.; Ba, Y.; Zhu, D.; Wang, G.; Qin, F. Effects of ECM proteins (laminin, fibronectin, and type IV collagen) on the biological behavior of Schwann cells and their roles in the process of remyelination after peripheral nerve injury. *Front. Bioeng. Biotechnol.* **2023**, *11*, 1133718. [CrossRef]
29. Yao, X.; Zhang, Y.; Hao, J.; Duan, H.Q.; Zhao, C.X.; Sun, C.; Li, B.O.; Fan, B.Y.; Wang, X.U.; Li, W.X.; et al. Deferoxamine promotes recovery of traumatic spinal cord injury by inhibiting ferroptosis. *Neural Regen. Res.* **2019**, *14*, 532–541, Erratum in *Neural Regen. Res.* **2019**, *14*, 1068. <https://doi.org/10.4103/1673-5374.250633>. [CrossRef]
30. De Mello, T.; Dunlop, S.; Plant, G.W. Myelination of axons by olfactory ensheathing glia. In Proceedings of the Fourteenth Annual Combined Biological Sciences Meeting, Copenhagen, The Netherlands, 15–18 April 2023; Newberry, J.A., Quail, E.A., Watson, M., Eds.; BioMed Chem: London, UK, 2003; Volume 1, p. 15.
31. Wang, X.; Wei, L.; Li, Q.; Lai, Y. HIF-1 α protects osteoblasts from ROS-induced apoptosis. *Free Radic. Res.* **2022**, *56*, 143–153. [CrossRef]
32. Yu, Y.; Yan, Y.; Niu, F.; Wang, Y.; Chen, X.; Su, G.; Liu, Y.; Zhao, X.; Qian, L.; Liu, P.; et al. Ferroptosis: A cell death connecting oxidative stress, inflammation and cardiovascular diseases. *Cell Death Discov.* **2021**, *7*, 193. [CrossRef]
33. Zheng, X.; Baker, H.; Hancock, W.S.; Fawaz, F.; McCaman, M.; Pungor, E., Jr. Proteomic analysis for the assessment of different lots of fetal bovine serum as a raw material for cell culture. Part IV. Application of proteomics to the manufacture of biological drugs. *Biotechnol. Prog.* **2006**, *22*, 1294–1300. [CrossRef]
34. Nakamura, M.; Okano, H. Cell transplantation therapies for spinal cord injury focusing on induced pluripotent stem cells. *Cell Res.* **2013**, *23*, 70–80. [CrossRef]
35. Schepici, G.; Gugliandolo, A.; Mazzon, E. Serum-Free Cultures: Could They Be a Future Direction to Improve Neuronal Differentiation of Mesenchymal Stromal Cells? *Int. J. Mol. Sci.* **2022**, *23*, 6391. [CrossRef] [PubMed]
36. Andersen, N.D.; Srinivas, S.; Piñero, G.; Monje, P.V. A rapid and versatile method for the isolation, purification and cryogenic storage of Schwann cells from adult rodent nerves. *Sci. Rep.* **2016**, *6*, 31781. [CrossRef] [PubMed]
37. Ravelo, K.M.; Andersen, N.D.; Monje, P.V. Magnetic-Activated Cell Sorting for the Fast and Efficient Separation of Human and Rodent Schwann Cells from Mixed Cell Populations. *Methods Mol. Biol.* **2018**, *1739*, 87–109. [CrossRef] [PubMed]
38. Skaper, S.D.; Manthorpe, M.; Adler, R.; Varon, S. Survival, proliferation and morphological specialization of mouse Schwann cells in a serum-free, fully defined medium. *J. Neurocytol.* **1980**, *9*, 683–697. [CrossRef]
39. Yan, H.; Bunge, M.B.; Wood, P.M.; Plant, G.W. Mitogenic response of adult rat olfactory ensheathing glia to four growth factors. *Glia* **2001**, *33*, 334–342. [CrossRef]
40. Haase, V.H. Hypoxic regulation of erythropoiesis and iron metabolism. *Am. J. Physiol.-Ren. Physiol.* **2010**, *299*, F1–F13. [CrossRef]
41. Kang, M.; Yang, Y.; Zhang, H.; Zhang, Y.; Wu, Y.; Denslin, V.; Othman, R.B.; Yang, Z.; Han, J. Comparative Analysis of Serum and Serum-Free Medium Cultured Mesenchymal Stromal Cells for Cartilage Repair. *Int. J. Mol. Sci.* **2024**, *25*, 10627. [CrossRef]
42. Chase, L.G.; Lakshminpathy, U.; Solchaga, L.A.; Rao, M.S.; Vemuri, M.C. A novel serum-free medium for the expansion of human mesenchymal stem cells. *Stem Cell Res. Ther.* **2010**, *1*, 8. [CrossRef]

43. Ito, D.; Fujita, N.; Ibanez, C.; Sasaki, N.; Franklin, R.J.; Jeffery, N.D. Serum-free medium provides a clinically relevant method to increase olfactory ensheathing cell numbers in olfactory mucosa cell culture. *Cell Transplant.* **2008**, *16*, 1021–1027. [[CrossRef](#)] [[PubMed](#)]
44. Gao, X.; Hu, G.; Fan, G.; Mei, Z.; Deng, L.; Du, J. Protective Effect of bFGF on Bone Marrow Mesenchymal Stem Cell against Hydrogen Peroxide-Induced Apoptosis. *Open Access Libr. J.* **2016**, *3*, 68251. [[CrossRef](#)]
45. David, B.T.; Curtin, J.J.; Brown, J.L.; Scorpio, K.; Kandaswamy, V.; Coutts, D.J.; Vivineto, A.; Bianchimano, P.; Karuppagounder, S.S.; Metcalfe, M.; et al. Temporary induction of hypoxic adaptations by preconditioning fails to enhance Schwann cell transplant survival after spinal cord injury. *Glia* **2023**, *71*, 648–666. [[CrossRef](#)] [[PubMed](#)]
46. Liu, S.; Yang, W.; Li, Y.; Sun, C. Fetal bovine serum, an important factor affecting the reproducibility of cell experiments. *Sci. Rep.* **2023**, *13*, 1942. [[CrossRef](#)]
47. Ayton, S.; Lei, P.; Mclean, C.; Bush, A.I.; Finkelstein, D.I. Transferrin protects against Parkinsonian neurotoxicity and is deficient in Parkinson's substantia nigra. *Signal Transduct. Target. Ther.* **2016**, *1*, 16015. [[CrossRef](#)]
48. Tacchini, L.; Bianchi, L.; Bernelli-Zazzera, A.; Cairo, G. Transferrin receptor induction by hypoxia. HIF-1-mediated transcriptional activation and cell-specific post-transcriptional regulation. *J. Biol. Chem.* **1999**, *274*, 24142–24146. [[CrossRef](#)]
49. Lee, J.H.; Yoo, J.Y.; Kim, H.B.; Yoo, H.I.; Song, D.Y.; Min, S.S.; Baik, T.K.; Woo, R.S. Neuregulin1 Attenuates H₂O₂-Induced Reductions in EAAC1 Protein Levels and Reduces H₂O₂-Induced Oxidative Stress. *Neurotox. Res.* **2019**, *35*, 401–409. [[CrossRef](#)]
50. Ahluwalia, A.; Tarnawski, A.S. Critical role of hypoxia sensor–HIF-1 α in VEGF gene activation. Implications for angiogenesis and tissue injury healing. *Curr. Med. Chem.* **2012**, *19*, 90–97. [[CrossRef](#)]
51. Sondell, M.; Lundborg, G.; Kanje, M. Vascular endothelial growth factor has neurotrophic activity and stimulates axonal outgrowth, enhancing cell survival and Schwann cell proliferation in the peripheral nervous system. *J. Neurosci.* **1999**, *19*, 5731–5740. [[CrossRef](#)]
52. Quarles, R.H. Myelin-associated glycoprotein (MAG): Past, present and beyond. *J. Neurochem.* **2007**, *100*, 1431–1448. [[CrossRef](#)]
53. Arellano-Carbalaj, F.; Briseño-Roa, L.; Couto, A.; Cheung, B.H.; Labouesse, M.; de Bono, M. Macoilin, a conserved nervous system-specific ER membrane protein that regulates neuronal excitability. *PLoS Genet.* **2011**, *7*, e1001341. [[CrossRef](#)] [[PubMed](#)]
54. Agthong, S.; Kaewsema, A.; Tanomsridejchai, N.; Chentanez, V. Activation of MAPK ERK in peripheral nerve after injury. *BMC Neurosci.* **2006**, *7*, 45. [[CrossRef](#)] [[PubMed](#)]
55. Kang, N.; Koo, J. Olfactory receptors in non-chemosensory tissues. *BMB Rep.* **2012**, *45*, 612–622. [[CrossRef](#)]
56. Flegel, C.; Manteniotis, S.; Osthold, S.; Hatt, H.; Gisselmann, G. Expression profile of ectopic olfactory receptors determined by deep sequencing. *PLoS ONE* **2013**, *8*, e55368. [[CrossRef](#)]
57. Korolchuk, V.I.; Menzies, F.M.; Rubinsztein, D.C. Mechanisms of cross-talk between the ubiquitin-proteasome and autophagy-lysosome systems. *FEBS Lett.* **2010**, *584*, 1393–1398. [[CrossRef](#)] [[PubMed](#)]
58. Glenn, T.D.; Talbot, W.S. Signals regulating myelination in peripheral nerves and the Schwann cell response to injury. *Curr. Opin. Neurobiol.* **2013**, *23*, 1041–1048. [[CrossRef](#)]
59. Luo, S.; Rubinsztein, D.C. BCL2L11/BIM: A novel molecular link between autophagy and apoptosis. *Autophagy* **2013**, *9*, 104–105. [[CrossRef](#)]
60. Xiang, J.; Liu, X.; Ren, J.; Chen, K.; Wang, H.L.; Miao, Y.Y.; Qi, M.M. How does estrogen work on autophagy? *Autophagy* **2019**, *15*, 197–211. [[CrossRef](#)]
61. Zhao, Y.; Klionsky, D.J.; Wang, X.; Huang, Q.; Deng, Z.; Xiang, J. The Estrogen-Autophagy Axis: Insights into Cytoprotection and Therapeutic Potential in Cancer and Infection. *Int. J. Mol. Sci.* **2024**, *25*, 12576. [[CrossRef](#)]
62. Monje, P.V.; Rendon, S.; Athauda, G.; Bates, M.; Wood, P.M.; Bunge, M.B. Non-antagonistic relationship between mitogenic factors and cAMP in adult Schwann cell re-differentiation. *Glia* **2009**, *57*, 947–961. [[CrossRef](#)]
63. Raschig, J.; Mailänder-Sánchez, D.; Berscheid, A.; Berger, J.; Strömstedt, A.A.; Courth, L.F.; Malek, N.P.; Brötz-Oesterhelt, H.; Wehkamp, J. Ubiquitously expressed Human Beta Defensin 1 (hBD1) forms bacteria-entrapping nets in a redox dependent mode of action. *PLoS Pathog.* **2017**, *13*, e1006261. [[CrossRef](#)] [[PubMed](#)]
64. Forrester, S.J.; Kikuchi, D.S.; Hernandez, M.S.; Xu, Q.; Griendling, K.K. Reactive Oxygen Species in Metabolic and Inflammatory Signaling. *Circ. Res.* **2018**, *122*, 877–902. [[CrossRef](#)]
65. Alves-Lopes, R.; Neves, K.B.; Strembitska, A.; Harvey, A.P.; Harvey, K.Y.; Yusuf, H.; Haniford, S.; Hepburn, R.T.; Dyet, J.; Beattie, W.; et al. Osteoprotegerin regulates vascular function through syndecan-1 and NADPH oxidase-derived reactive oxygen species. *Clin. Sci.* **2021**, *135*, 2429–2444. [[CrossRef](#)]
66. Rochette, L.; Meloux, A.; Rigal, E.; Zeller, M.; Cottin, Y.; Vergely, C. The Role of Osteoprotegerin and Its Ligands in Vascular Function. *Int. J. Mol. Sci.* **2019**, *20*, 705. [[CrossRef](#)] [[PubMed](#)]
67. Dai, Y.; Grant, S. BCL2L11/Bim as a dual-agent regulating autophagy and apoptosis in drug resistance. *Autophagy* **2015**, *11*, 416–418. [[CrossRef](#)] [[PubMed](#)]
68. Marquez, R.T.; Xu, L. Bcl-2:Beclin 1 complex: Multiple, mechanisms regulating autophagy/apoptosis toggle switch. *Am. J. Cancer Res.* **2012**, *2*, 214–221.

69. Gelman, A.; Rawet-Slobodkin, M.; Elazar, Z. Huntingtin facilitates selective autophagy. *Nat. Cell Biol.* **2015**, *17*, 214–215. [[CrossRef](#)]
70. Hoffman, L.M.; Jensen, C.C.; Beckerle, M.C. Phosphorylation of the small heat shock protein HspB1 regulates cytoskeletal recruitment and cell motility. *Mol. Biol. Cell* **2022**, *33*, ar100. [[CrossRef](#)]
71. Yan, L.; Li, Z.; Li, C.; Chen, J.; Zhou, X.; Cui, J.; Liu, P.; Shen, C.; Chen, C.; Hong, H.; et al. Hspb1 and Lgals3 in spinal neurons are closely associated with autophagy following excitotoxicity based on machine learning algorithms. *PLoS ONE* **2024**, *19*, e0303235. [[CrossRef](#)]
72. Feng, J.; Fu, S.; Cao, X.; Wu, H.; Lu, J.; Zeng, M.; Liu, L.; Yang, X.; Shen, Y. Synaptonemal complex protein 2 (SYCP2) mediates the association of the centromere with the synaptonemal complex. *Protein Cell* **2017**, *8*, 538–543. [[CrossRef](#)]
73. Yamamoto, S.; Kuramoto, K.; Wang, N.; Situ, X.; Priyadarshini, M.; Zhang, W.; Cordoba-Chacon, J.; Layden, B.T.; He, C. Autophagy Differentially Regulates Insulin Production and Insulin Sensitivity. *Cell Rep.* **2018**, *23*, 3286–3299. [[CrossRef](#)] [[PubMed](#)]
74. Huang, B.; Wei, W.; Wang, G.; Gaertig, M.A.; Feng, Y.; Wang, W.; Li, X.J.; Li, S. Mutant huntingtin downregulates myelin regulatory factor-mediated myelin gene expression and affects mature oligodendrocytes. *Neuron* **2015**, *85*, 1212–1226. [[CrossRef](#)] [[PubMed](#)]

Disclaimer/Publisher’s Note: The statements, opinions and data contained in all publications are solely those of the individual author(s) and contributor(s) and not of MDPI and/or the editor(s). MDPI and/or the editor(s) disclaim responsibility for any injury to people or property resulting from any ideas, methods, instructions or products referred to in the content.